EMPIRICAL GROUND-MOTION RELATIONS FOR SUBDUCTION ZONE EARTHQUAKES AND THEIR APPLICATION TO CASCADIA AND OTHER REGIONS

Gail M. Atkinson and David M. Boore

For submission to Bull. Seism. Soc. Am.: Oct. 04, 2002

ABSTRACT

Ground-motion relations for earthquakes that occur in subduction zones are an important input to seismic-hazard analyses in many parts of the world. In the Cascadia region (Washington, Oregon and British Columbia), for example, there is a significant hazard from megathrust earthquakes along the subduction interface and from large events within the subducting . We have compiled a response spectra database from thousands of strong motion recordings from events of moment magnitude (**M**) 5 to 8.3 occurring in subduction zones around the world, including both interface and in-slab events. The 2001 Nisqually and 1999 Satsop earthquakes are included in the database, as are many records from subduction zones in Japan (KNET data), Mexico (Guerrero data), and Central America. The size of the database is much larger than that available for previous empirical regressions to determine ground-motion relations for subduction zone earthquakes. The large dataset enables improved determination of attenuation parameters and magnitude scaling, for both interface and in-slab events. Soil response parameters are also better determined by the data.

We use the database to develop global ground-motion relations for interface and in-slab earthquakes, using a maximum-likelihood regression method. We analyze regional variability of ground-motion amplitudes across the global database, and find that there are significant regional differences. In particular, amplitudes in Cascadia differ by more than a factor of two from those in Japan for the same magnitude, distance, event type, and NEHRP site class. This is believed to be due to regional differences in the depth of the soil profile, that are not captured by the NEHRP site classification scheme. Regional correction factors to account for these differences are proposed for Cascadia and Japan.

The results of this study differ significantly from previous analyses based on more limited data, and have important implications for seismic-hazard analysis. The ground-motion relations predict that

a great megathrust earthquake (**M** ≥8) at a fault distance of about 100 km would produce PSA on soil sites of about 110 cm/s^2 at 0.5 Hz, 660 cm/s^2 at 2.5 Hz and 410 cm/s^2 at 5 Hz, with a peak ground acceleration of about 18%g. These damaging levels of motion would be experienced over a very large area, corresponding to a rectangle about 300 km wide by 500 km long. Large in-slab events (**M** 7.5) would produce even higher PSA values within 100 km of the fault, but the in-slab motions attenuate much more rapidly with distance, greatly reducing the damage potential of in-slab events like the Nisqually earthquake, relative to a mega-thrust event. This is true not only for low-frequency ground motion, but even for 5 Hz. This suggests that the contemporary view of seismic hazard, namely that in-slab events dominate the hazard for 5 Hz for the 2% in 50 year probability level, may need revision. The hazard posed by moderate-to-large in-slab events such as the 2001 Nisqually earthquake is modest compared to that of a Cascadia mega-thrust earthquake of **M** ≥ 8, in terms of the area that would experience damaging levels of ground motion.

INTRODUCTION

Ground-motion relations for earthquakes that occur in subduction zones are an important input to seismic-hazard analyses for the Cascadia region (Washington, Oregon and British Columbia). There is a significant hazard from mega-thrust earthquakes along the subduction interface, and from large events within the subducting slab. We refer to these types of earthquakes as interface and in-slab, respectively. Despite recent moderate in-slab earthquakes in Washington, such as the 2001 Nisqually and 1999 Satsop events, there remains a paucity of ground-motion data in the Cascadia region from which to develop regression relations. Therefore it is common practice in regional seismic-hazard analyses to employ empirical ground-motion relations based on a global subduction database. For example, the national seismic-hazard maps developed by both the U.S. Geological Survey (Frankel et al., 1996) and the Geological Survey of Canada (Adams et al., 1999), and incorporated into current building code provisions, model the ground motions from in-slab and interface earthquakes using the global subduction relationships developed by Youngs et al. (1997). Preliminary studies of limited empirical databases have suggested that there are no detectable differences between ground motions amongst different subduction regions, for a given magnitude and distance (Atkinson, 1997). Thus it would appear that the collation of data from different subduction regimes around the world into a single database for regression analyses is both necessary and reasonable. This assumption is one of many that will be tested in this study.

We have compiled a response spectra database from thousands of ground-motion recordings from events of moment magnitude (**M**) 5 to 8.3 occurring in subduction zones around the world, including both interface and in-slab events. The 2001 Nisqually and 1999 Satsop earthquakes are included in the database, as are many records from subduction zones in Japan (KNET data), Mexico (Guerrero data), and Central America. The size of the database is much larger than that used in previous regressions for subduction zone earthquakes. For example, the Youngs et al. (1997) database contains 350 horizontal-component response spectra, compiled for earthquakes occurring through 1989. The new database, compiled for earthquakes occurring through 2001, contains 1200 horizontal-component spectra in the magnitude-distance range of interest for regression (eg. roughly **M**>5 within 100 km, or **M**>7 within 300 km), plus many thousand more records for greater distances that can be used to explore various aspects of the ground-motion scaling with magnitude and distance. All spectra are horizontal component, for 5% of critical damping. The large dataset enables better determination of attenuation parameters and magnitude scaling, for both types of events, than has previously been possible. Soil response parameters are also better determined by the data. The new data suggest that significant revisions to current estimates of seismic hazard may be required.

DATABASE FOR REGRESSION

The database for regression builds on past work and adds many new ground-motion recordings that have become available in the last decade. The Youngs et al. (1997) global subduction database was compiled in about 1989 by adding to an early version of the subduction database compiled by Crouse (1991). Thus the Crouse (1991) catalogue contains events not in the Youngs et al. (1997) catalogue, and vice versa. We therefore began by merging the global subduction databases compiled by Crouse (1991) and Youngs et al. (1997) to create a single historical subduction database containing records from subduction zones around the world through 1989. We then added readily-available data from more recent in-slab and interface events. These included events in Cascadia (strong-motion and broadband seismographic records), Japan (KNET strong-motion data), Mexico (Guerrero strong-motion data) and Central America (El Salvador strong-motion data). The compiled database forms an electronic supplement to this paper (http://www.seismosoc.org/publications/bssa-esupps.html). For each record, the database lists the moment magnitude, as obtained from the historical database or from a search of the Harvard CMT or Japanese FREESIA websites; focal mechanism information and depths were also obtained from these sources. The tabulated distance measure in the database is the closest distance to the earthquake fault plane. For events in the Youngs et al. database, we adopted

these values directly from their database. For the Crouse et al. database, we estimated the closest fault distance based on the epicentral distance and the event magnitude, assuming that:

1. the size of the fault plane is given by the empirical relationships of Wells and Coppersmith (1994) that predict fault length and area as a function of moment magnitude; and
2. the epicenter lies above the geometric center of a dipping fault plane.

For recent events of moderate magnitude, we also used the epicentral distance and event magnitude to estimate closest distance to fault (in the same way as described above). We checked that this approach provides reasonable estimates of the closest fault distance on average, by plotting these estimated closest fault distances against actual values for several large events for which the fault geometry is known.

The event classification by type was based on both focal depth and mechanism. Event location and depth were first used to establish that the event was a subduction event (ie. either interface or in-slab). Amongst the subduction events, normal fault mechanisms are always in-slab events. Thrust mechanisms imply interface events for earthquakes that occur at depths of less than 50 km on shallow dipping planes; in this depth range the subducting oceanic plate is in contact with the over-riding continental crust. Thrust mechanisms are assumed to represent in-slab events if the events occur at depths greater than 50 km (ie. below the crustal contact zone), or if they occur on steeply dipping planes. Events of unknown type are not included in the regression, nor are events of focal depth greater than 100 km. Events that occur within the crust, above the subduction zone, are not included in the database.

Each record is assigned a NEHRP site class (see Dobry et al., 2000). For the recent Japanese data, the classification was based on the shear-wave velocity profiles of the sites, as determined by borehole measurements. The procedure used to assign NEHRP site classes based on the KNET borehole information is described in the Appendix. For the Guerrero data, the sites are all classified as rock, which we have assumed equivalent to NEHRP B (J. Anderson, pers. comm., 1999; Chen and Atkinson, 2002). Broadband stations in Washington and British Columbia (B.C.) are also sited on rock. We assume that these sites are best classed as NEHRP B; the assumed average shear-wave velocity is about 1100 m/s (see Atkinson and Cassidy, 2000). Strong-motion sites in Washington are largely soil, and have been classified using a map of site classes prepared by R. Haugerud (written commun., 2001). The map was based on surficial geology, using correlations between the geology and the average shear-wave velocity to 30 m from data in Washington. Blind comparisons of the site classes predicted from his map with those from 8 sites with actual shear-wave velocity measurements (Williams et al., 1999; R. Williams, written commun., 2001) were in excellent agreement. For the

historical data in the Youngs et al. catalogue, the assigned Geomatrix classification scheme was converted to the NEHRP equivalent by assuming Geomatrix A = NEHRP B, Geomatrix B = NEHRP C, Geomatrix C/D = NEHRP D and Geomatrix E = NEHRP E. This equivalence is based on shear-wave velocities and descriptions quoted for the Geomatrix classification scheme (eg. Abrahamson and Silva, 1997).

The distribution of the database used in the regressions is shown on Figure 1 for both in-slab and interface events. The database is available in digital form from the electronic supplement to this paper (www.seismosoc.org). Observe on Figure 1 that the data are relatively plentiful in the most important magnitude-distance ranges. Specifically, we are most interested in two 'design earthquake' scenarios that contribute most to seismic hazard in the Cascadia region, according to deaggregations of typical hazard results (eg. Frankel et al., 1999). These are (i) in-slab earthquakes of **M** 6.5 to 7.5 at fault distances of 40 to 100 km (since events are within the slab at depths that are typically 50 km or more, fault distances will nearly always exceed 40 km); and (ii) interface earthquakes of **M**≥7.5 at fault distances of 20 to 200 km (typical depths of about 20 km). It is the in-slab events that have multiplied within the database most markedly in recent years, particularly with the occurrence of the 2001 Nisqually, Washington and 2001 Geiyo, Japan events of **M** 6.8.

Records from moderate events at large distances recorded on the KNET network in Japan are not reliable at higher frequencies due to limitations of the instrumentation (Heenan, 2002). To ensure that all analyses are well within the reliable range, the KNET data are excluded from the regressions for events of **M**<6 at distances beyond 100 km; for larger events the KNET data are not used for distances beyond 200 km. KNET data outside of the reliable range are not shown on Figure 1. These data may be useful at lower frequencies but we have eliminated them from the regressions due to the potential problems at higher frequencies.

REGRESSION ANALYSIS

Functional Form

Regression of the dataset has been performed using the maximum-likelihood method (Joyner and Boore, 1993, 1994). Separate regressions are performed for the interface and in-slab events, since our analyses indicated that there are extensive differences in the amplitudes, scaling, and attenuation of these different event types. After detailed experimentation with a variety of function forms, the adopted functional form (all logs base 10) is:

$$\log Y = c_1 + c_2 \mathbf{M} + c_3 h + c_4 R - g \log R + c_5 sl\ S_C + c_6 sl\ S_D + c_7 sl\ S_E \qquad (1)$$

where:

Y is peak ground acceleration (PGA) or 5% damped pseudo-acceleration (PSA) in cm/s^2, random horizontal component

M = moment magnitude (use **M**=8.5 for interface events of **M**>8.5, **M**=8.0 for in-slab events of **M**≥8)

h = focal depth in km, $R = \sqrt{(D_{fault}^2 + \Delta^2)}$ with D_{fault} = closest distance to fault surface, in km (use h=100 km for events with depth > 100 km)

$\Delta = 0.00724\ 10^{0.507\ \mathbf{M}}$

S_C=1 for NEHRP C soils (360<β≤760 m/s), =0 otherwise

S_D=1 for NEHRP D soils (180≤β≤360 m/s), =0 otherwise

S_E=1 for NEHRP E soils (β<180 m/s), =0 otherwise

$g = 10^{(1.2 - 0.18\ \mathbf{M})}$ for interface events, $g = 10^{(0.301 - 0.01\ \mathbf{M})}$ for in-slab events

sl = 1.	for PGArx≤ 100 cm/s^2 OR frequencies ≤ 1 Hz
sl = 1. – (f-1) (PGArx-100.)/400.	for 100.<PGArx<500. cm/s^2 (1 Hz<f<2 Hz)
sl = 1. - (f-1)	for PGArx≥500. cm/s^2 (1 Hz<f<2 Hz.)
sl = 1. – (PGArx-100.)/400.	for 100.<PGArx<500. cm/s^2 (f≥2 Hz)
sl = 0.	for PGArx≥500. cm/s^2 (f≥2 Hz)

PGArx = predicted PGA on rock (NEHRP B), in cm/s^2

σ = standard deviation of residuals = $\sqrt{(\sigma_1^2 + \sigma_2^2)}$ where 1, 2 denote estimated intra-event and inter-event variability, respectively. Note that β is the shear-wave velocity averaged over the top 30m of the soil profile.

The selected functional form incorporates the results of analyses into specific features of the data, such as the magnitude dependence of the geometrical spreading coefficient *g*, the functional form for the scaling of amplitudes with magnitude, and amplitude-dependent soil nonlinearity, as described below. There are attributes of this functional form that may be considered unusual. The distance variable for regression, R, is approximately equal to the average distance to the fault surface. The Δ term that combines with D_{fault} to form R is defined from basic fault-to-site geometry: for a fault with length and width given by the empirical relations of Wells and Coppersmith (1993) for all fault types, the average distance to the fault for a specified D_{fault} is calculated (arithmetically averaged from a number of points distributed around the fault), then used to determine Δ, which is a function of fault size. Thus the distance measure depends on the closest distance to the fault and the earthquake magnitude; the magnitude-dependence of R arises because large events have a large spatial extent, so that even near-fault observation points are far away from most of the fault. It is important to note that

the coefficients that appear in the definition of Δ were defined analytically, so as to represent average fault distance. They were not determined by the regression. However, trial regressions were performed to verify that alternative definitions of the distance measure (using different coefficients to define Δ, over a wide range of possible values) would not result in improved accuracy of model predictions, relative to the average-fault-distance measure that we selected.

The magnitude dependence of the geometric spreading coefficient *g* was determined by preliminary regressions of the data for both interface and in-slab events. These preliminary regressions looked at slices of data in 1-unit magnitude increments (eg. $5 \le \mathbf{M} < 6$, $5.2 \le \mathbf{M} < 6.2$, etc.) to determine the slope of the attenuation as a function of magnitude. For this exercise, we looked only at the low-frequency (0.5 and 1 Hz) PSA data, within the distance range from 50 to 300 km. (Note: we use data at closer distances for the final regressions.) The selection of data with $D_{fault} \ge 50$ km was made to avoid near-source distance saturation effects, which are handled by the Δ term. For the data within each magnitude bin, the regression was made to a simple functional form, given by:

$$\text{Log } Y' = a_1 + a_2 \mathbf{M} - g \log R + a_3 S \qquad (2)$$

where Y' is the PSA for 0.5 Hz or 1 Hz, corrected for curvature of the attenuation line due to anelasticity assuming $Y' = Y \exp(0.001R)$, R is the average distance to the fault as defined in Equation (1), and S = 0 for rock (A, B) or 1 for soil (C, D, E). The coefficient *g* is the far-field slope determined for each magnitude bin. As illustrated on Figure 2, the obtained values of the attenuation slope were plotted as a function of magnitude to obtain the form assigned to *g* in the final regression. Note that there is a marked difference in the slope of the attenuation for interface and in-slab events, with the interface events showing a much more pronounced magnitude dependence to the attenuation. This contrast in attenuation behavior between interface and in-slab events is readily apparent in plots of data amplitudes, even without doing any regression analyses. This is illustrated in Figure 3. The very flat attenuation of large interface events relative to large in-slab events has important implications for the relative impact of these two types of events on seismic hazard. It is evident that large interface events will cause damaging ground motions over a much greater area than will large in-slab events.

The soil response terms in the final regression include both linear and nonlinear effects. Nonlinear soil effects are not strongly apparent in the database or upon examination of the residuals from preliminary regression results, as most records have PGA<200 cm/s^2, but may be important in using the relations for the largest magnitudes and closest distances. To determine the linear soil effects, we performed separate preliminary regressions of each dataset (interface and in-slab) to determine the coefficients c_5, c_6 and c_7 (assuming linear soil response). We used these preliminary results, weighted

by the number of observations in each of the two datasets, then smoothed, to assign fixed values to c_5, c_6 and c_7 (independent of earthquake type) for subsequent regressions. The reason that we fix these terms for the final regressions is to ensure that the soil response coefficients are equal for the in-slab and interface datasets. The soil linearity term, *sl*, was assigned by looking for evidence of nonlinearity in residual plots from these preliminary regressions and from consideration of the NEHRP guidelines for nonlinearity (Dobry et al., 2000). We concluded that there is weak evidence of nonlinearity in the dataset for records with PGA_{rx}>100 cm/s^2, for E soils at frequencies above 1 Hz, and that the data are consistent with the concept that soil and rock amplitudes converge at high amplitudes. Based on these observations and the factors suggested by NEHRP, we assume that the soil coefficients may be multiplied by a soil linearity factor that decreases from a value of 1.0 (fully linear) at PGA_{rx} =100 cm/s^2 to a value of 0.0 (fully nonlinear) at PGA_{rx} =500 cm/s^2. This scheme was used to fix the term *sl* for the final regressions, using the form given in Equation 1. Figure 4 shows the soil coefficients c_5, c_6 and c_7 for NEHRP site classes C, D and E, respectively, and their dependence on PGA_{rx}.

The final regression is performed by taking all terms with fixed coefficients to the left side of the equation; thus we add $g \log R + c_5\, sl\ S_C + c_6\, sl\ S_D + c_7\, sl\ S_E$ to log Y before regression to determine the remaining coefficients. This process needs to be iterated a few times because the resulting PGA_{rx} is used in the definition of the dependent variable for the regression. After a few iterations, the coefficients for PGA_{rx} remain unchanged by further iteration and the regression is complete.

In order to optimize the fit for the magnitude-distance range of engineering interest we limited the final regression to data that fell within the following criteria (where D_{fault} is the closest distance to the fault):

Interface events:

5.5 ≤**M**<6.5 D_{fault} ≤80 km

6.5≤**M**<7.5 D_{fault} ≤150 km

M≥7.5 D_{fault} ≤300 km

In-slab events:

6.0≤**M**<6.5 D_{fault} ≤100 km

M≥6.5 D_{fault} ≤200 km

These criteria were refined by experimenting with the regression results until an optimal fit of the regression equation to the data was achieved for the events that are important to seismic-hazard analysis: namely interface events of **M**≥7.5 and in-slab events of **M**≥6.5, at distances of up to 200 km,

as well as smaller earthquakes at close distances. The need to restrict the magnitude-distance range for regression arises from the fact that there are many more data recorded for moderate events and intermediate distances than for large events and close distances. Thus the database is dominated by the former, while the hazard is dominated by the latter. This needs to be considered in selection of the data for regression, in order to avoid a result that is dominated by data availability. The larger database is still useful in exploring several aspects of the functional form, such as those discussed above, and in quantifying the fit of the relations in the magnitude-distance ranges not specifically included in the final regressions.

Finally, after performing the regressions to the selected functional form, the resulting coefficients were lightly smoothed (using a weighted 3-point smoothing) over frequency. This ensures a smooth spectral shape against frequency and allows for reliable interpolation of coefficients for frequency values not explicitly used in the regression.

In our initial regressions, a quadratic term in magnitude was used to model the scaling of amplitudes with magnitude: our initial form had a term in $\mathbf{M}^2$ as well as in **M**. The quadratic term leads to a better fit than the linear magnitude scaling overall, but the sign of the quadratic term is positive, rather than negative as would be expected. To ensure the best fit in the magnitude range that is both important to hazard and constrained by data, while providing realistic scaling outside of this range, the quadratic source terms in the equation were refit to a linear form. The linear model was constrained to provide the same results in the magnitude range from 7.0 to 8.0 for interface events and from 6.5 to 7.5 for in-slab events. Thus the initial source description of $[c_1' + c_2' (\mathbf{M}\text{-}6) + c_3'(\mathbf{M}\text{-}6)^2]$ was refit to $[c_1 + c_2 \mathbf{M}]$. The scaling of amplitudes with magnitude for near and far distances, for both the initial quadratic and the adopted linear form, is shown in Figures 5 to 8, for interface and in-slab events. The curvature displayed for the linear magnitude scaling results from the interplay of the magnitude-dependent slope of the attenuation with the magnitude scaling. From these plots, it is apparent that the ground-motion relations require the imposition of a maximum magnitude of 8.5 for prediction of interface amplitudes, or 8.0 for prediction of in-slab amplitudes. At greater magnitudes (beyond the range of the data), the predicted amplitudes will grow smaller rather than larger. Thus estimates of ground motion for interface events of $\mathbf{M}>8.5$ should be made using $\mathbf{M}=8.5$, while estimates of ground motion for in-slab events of $\mathbf{M}>8.0$ should be made using $\mathbf{M}=8.0$. Restrictions should also be placed on the depth term, to prevent the prediction of unrealistically large amplitudes for earthquakes deeper than the 100 km depth cut-off applied in the regressions. If the equations are extrapolated for depths > 100 km, a value of h=100 km should be assumed.

Results

The coefficients of the regression are given in Table 1. Values for other frequencies can be obtained by linear interpolation of each coefficient value in log frequency space. Inspection of the coefficients c_5 through c_7 reveals that soil motions exceed rock motions by as much as a factor of four for soft soils at low frequencies. There is a weak depth effect given by the coefficient c_3, with deeper events causing larger motions.

The recommended standard deviation of the residuals is also listed in Table 1. The values of σ listed in Table 1 are calculated based on records within 100 km of the fault, considering all soil types. For interface events, the standard deviation is calculated considering all events of **M** ≥7.2, while for in-slab events it is calculated considering all events of **M** ≥6.5. These magnitude ranges were selected in order to obtain the variability that is applicable to the magnitude ranges most relevant to hazard calculations. In a separate study, Atkinson and Casey (2002) have found that the KNET data from Japan appear to have a greater high-frequency site response than data of the same soil class from other regions, due to the prevalence of sites in Japan with shallow soil over rock. Thus their inclusion could artificially inflate the expected scatter of high-frequency amplitudes in any one region. For this reason the KNET data are not used in computing the standard deviation of residuals listed in Table 1. The regional variability of ground-motion residuals due to gross regional differences in site characteristics is evaluated in more detail below.

A rough estimate of how much of the total variability (σ) is attributable to intra-event variability(σ_1) is made by calculating this value for several of the larger-magnitude events for which the data are most plentiful, and determining an average value. The inter-event variability (σ_2) is then calculated assuming that $\sigma = \sqrt{(\sigma_1^2 + \sigma_2^2)}$.

Figure 9 compares peak ground acceleration (PGA) on rock and soil sites for both interface and in-slab events. Nonlinearity of soil response is important for records with $PGA_{rx} > 100$ cm/s^2 and will thus influence near-source observations of interface events of **M**≥7.5 or in-slab events of **M**>6.5.

Figure 10 plots in-slab versus interface ground motions on NEHRP D sites for frequencies of 0.5 Hz and 5 Hz for a moment magnitudes of 6.5, in comparison to the previous regression results of Youngs et al. (1997). Interface ground motions for **M** 8.5 are also shown. Our results are similar to those of Youngs et al. for the largest interface events, for which our databases are similar, but differ greatly for events of **M** 6.5, for which we have many more data. Note the very slow attenuation for great interface events in comparison to moderate in-slab events.

Great interface events pose a hazard to large areas because of the lack of significant attenuation within 300 km of the fault plane. In-slab events, by contrast, produce large near-source amplitudes; near-source amplitudes of in-slab events of **M** 7.5 are greater than those from interface amplitudes for events of **M** 8.5, by about a factor of two. However, the in-slab amplitudes attenuate rapidly with distance from the fault, resulting in hazard to a much smaller area. The finding of significantly different attenuation rates for in-slab versus interface events is a novel result of this analysis, with significant implications for seismic-hazard analysis.

EVALUATION OF RESULTS

The most relevant measure of any empirical regression result is how accurately it models the database that it purports to represent. With the large database available, we are able to present a more comprehensive analysis of the residuals than has been given in any previous regression studies for subduction-zone earthquakes. We have analyzed the residuals for both interface and in-slab events in a number of ways. (The residual is measured in log (base 10) units, and is defined as the difference between the log of the observed value and the log of the predicted value; thus a residual of +0.1 represents an underprediction by a factor of 1.26, for example.) Figure 11 shows the interface residuals as a function of distance, in three magnitude ranges, while Figure 12 shows the corresponding plot for in-slab events. In making these plots, all records of **M**≥5.5 in the database within 200 km of the fault were used, while for the large events (**M**≥6.5) all records within 300 km were used (including data from all regions). Note that this is a larger distance range than that used in the regressions, to enable a broader sense of how well the equations represent the larger database. Thus we don't necessarily expect zero average residuals over all magnitude and distance ranges. The residual plots indicate a large amount of random variability in the data. Overall, the average residuals are near zero for both types of events in the important distance range within 100 km of the fault (with some exceptions).

The standard deviation of the residuals (σ) for records of **M** ≥ 6 within 100 km of the fault is shown on Figure 13 as a function of frequency (using data from all regions). The random variability is an important parameter for seismic-hazard analysis. Overall, the variability is similar for interface and in-slab events. There is a significant tendency to lower variability for higher magnitudes (**M** ≥7.2). The standard deviation of the residuals is typically in the range from 0.2 to 0.35 log units for the larger events and 0.25 to 0.4 for the smaller events.

Figures 14 and 15 compare the predictions of the regression to the observed ground-motion amplitudes, at a range of frequencies, for the largest events that are well represented in the database.

These are interface earthquakes of **M** 8 ± 0.3 (there are no larger events in the database) and in-slab earthquakes of **M** 6.8 ± 0.3. In these figures, the predictions of our regression equations are plotted for the central magnitude value, for NEHRP B (rock) and D (soil). The corresponding predictions of the Youngs et al. (1997) relations are also shown. For large interface events, our predictions do not differ greatly from those of Youngs et al., and both sets of relations fit the data to about the same degree. For in-slab events we predict a significantly faster decay of amplitudes with distance than does the Youngs et al. relations, and this is clearly supported by the data. The much slower attenuation of ground-motion amplitudes for mega-thrust earthquakes as compared to moderate-to-large in-slab earthquakes is apparent in comparing Figure 14 to Figure 15.

The Youngs et al. (1997) relations were the first ground-motion relations to recognize the difference between in-slab and interface amplitudes, and have been widely used in engineering practice, including in the development of current seismic-hazard maps for building code applications. The Youngs et al. study followed a similar regression methodology to that used in this paper, based on maximum likelihood. There are two reasons for the differences between our results and theirs. First, they used a different functional form, and thus the relations may behave quite differently in the magnitude-distance ranges that are not well constrained by data. The second and more important reason for the differences lies in the increased database that we were able to employ: we had twelve more years of records, representing an order-of-magnitude increase in database size, particularly for the in-slab events. This enables us to more accurately distinguish differences in the amplitudes and distance-dependence of in-slab and interface events, as well as to more accurately model other effects such as the magnitude-dependence of attenuation, and soil response**.**

Figure 16 plots the predicted spectral amplitudes for moderate-to-large interface and in-slab events, at distances of 50 km and 100 km. For reference, the corresponding predictions for shallow crustal earthquakes in California (from Atkinson and Silva, 2000) are also shown. All relations are plotted for NEHRP C sites. Observe that at large magnitudes (**M** > 7) the in-slab motions are higher than the corresponding California crustal motions by more than a factor of two at most frequencies. By contrast, the interface motions for large events are broadly similar to those for California crustal events of a similar size and distance.

Analysis of Ground-motion Residuals by Magnitude, Soil Type and Region

To examine whether the large data variability includes systematic over- or under-prediction of records from certain regions or soil types, we examined figures and statistics showing subsets of the

data plotted in Figures 11 and 12, broken down by magnitude, soil type, and region. Table 2 summarizes the mean residuals, for records of **M** ≥ 6 within 100 km of the fault, for both interface and in-slab events. Examination of this table shows that there are significant positive residuals (denoting underprediction) for events of **M** < 6.6. This is attributable to our decision to force a linear scaling of amplitudes with magnitude, despite apparently high amplitudes at low magnitudes that would suggest a positive quadratic scaling (see figures 5 to 8). The positive residuals are considered acceptable because this magnitude range is below that which contributes most strongly to hazard. For larger magnitudes, the fit to the data is excellent.

Looking at the breakdown of residuals by site class, there are large positive residuals for Class C sites for interface events; most of these records are from Japan. However the Class C residuals for in-slab events, which are from both Japan and Cascadia, do not show this trend. For other site classes, there are no overwhelming trends, except that positive residuals for E sites at high frequencies from interface events appear to be balanced by negative residuals for in-slab events. The reason for the positive residuals for interface events on NEHRP C sites will soon become apparent, as we examine regional variability of residuals.

The breakdown of residuals by region shows that the Cascadia in-slab data tend to have positive residuals at lower frequencies, with negative residuals at higher frequencies. This is balanced out by the reverse trend in the Japan in-slab data. A detailed analysis of the **M** 6.8 2001 Nisqually, Washington earthquake versus the **M** 6.8 2001 Geiyo, Japan records suggests that this is likely due to differences in typical soil profiles, resulting in systematic regional differences in site amplification within the same NEHRP class (Atkinson and Casey, 2002). Sites in Japan, of all NEHRP classes, are typically shallow soil over rock, which tends to amplify high frequencies. In the Cascadia region, the NEHRP A/B classes represent rock or glacial till, while the NEHRP C/D/E classes represent relatively deep layers over rock or till. Computation of theoretical amplification functions for typical generic soil profiles for each region, using the method of Boore and Joyner (1997), indicates that sites in Japan are expected to have larger amplifications at high frequencies, while sites in Cascadia will have larger amplifications at low frequencies (Atkinson and Casey, 2002).

The high positive residuals for interface events in some of the breakdowns are influenced by inclusion of the 1992 Cape Mendocino, California earthquake of **M** 7.1 in our subduction-zone earthquake database (the residuals from this event are identified in Figure 11). We initially classified this as an interface event and thus included it in our analyses. However, there are arguments that could be made for treating it as a shallow crustal event. The argument in favor of considering it as an interface event is that the projection of the fault plane crops out near the seaward edge of the

subduction zone. On the other hand, this may be a crustal event because it was significantly shallower than the pre-earthquake seismicity in the area, and occurred in a volume having seismic velocities that match crustal velocities rather than subducted Gorda plate velocities (Oppenheimer et al., 2002). Thus it may be that this event is not really representative of interface events, but might be more nearly considered a California crustal earthquake (this is the only California earthquake in the database). Excluding the Cape Mendocino event from the database has only a minor effect on the regression, reducing the predictions somewhat for interface events of $\mathbf{M} < 7.5$.

In Figure 17 the regional variability of the ground-motion residuals is examined more closely, combining residuals from all records of $\mathbf{M} \geq 6$ within 100 km of the fault for both interface and in-slab events, for all soil types. The average residual over all regions is near zero, but does not equal zero at all frequencies since this data range does not exactly match that used in the regressions. Relative to this average, the Cascadia region residuals are noticeably positive at low frequencies, and noticeably negative at high frequencies. By contrast, the Japan residuals show the opposite trend. For other regions, the averages are not much different from zero (some of these regions have a very limited number of records). As discussed above, the opposing trends for Japan versus Cascadia can be attributed to regional differences in the depth of typical soil profiles. This points to a limitation of the NEHRP site classes in characterizing the soil types; the NEHRP classes capture the amplification effects due to the average shear wave velocity, but not its frequency-dependence due to the depth of the soil profile. Consequently, there are limitations on the applicability of global relations such as this one to any specific region. It is preferable to develop relations using data just from the region of interest. When that is not possible due to limitations of the database, an alternative would be to first adjust all recordings to a common site condition using regional soil amplification factors, prior to regression. If these factors are not known in advance, they can be determined from analysis of the residuals, as has been done here. In this case, the applicability of the relations to a specific region may be improved by using these average residuals as regional correction factors. Table 3 lists such regional correction factors for Cascadia and Japan. They were derived by subtracting the average residual over all regions from the corresponding residual for the specified region. To implement these correction factors, they should be added to the c_1 coefficients of Table 1. The revised c_1 coefficients that result are listed in Table 3.

As a final check on these adjusted equations, we replot the residuals for in-slab events by region, after applying the regional correction factors to Cascadia and Japan, as shown on Figure 18. The residuals for both Cascadia and Japan are acceptable, although there are still some low-amplitude residuals for Cascadia events of $\mathbf{M} < 6.5$ at high frequencies (mostly from the Satsop event). Table 4

provides statistics on the region-adjusted residuals (data from all regions are included) for the magnitude-distance range of most interest to hazard analysis: **M**≥7.5 at D_{fault}<300 km for interface events and **M**≥6.5 at D_{fault}<100 km for in-slab events. Note that in some cases the standard deviation has been reduced from that quoted in Table 1, due to the slightly different magnitude-distance criteria applied for selection of records and due to the application of the regional factors for Cascadia and Japan. In a few instances the standard deviation is slightly higher due to the broader distance range considered for the interface events. The user may select either set of standard deviations (Table 1 or Table 4) depending on which better matches the magnitude-distance range of interest for their application. The intra-event component of variability (σ_1) would be the same in either case.

CONCLUSIONS

We have presented ground-motion relations for interface and in-slab earthquakes based on regression of a large global database, containing thousands of ground-motion records for events of **M**≥5 at distances up to several hundred km. The results of this study differ significantly from previous analyses based on more limited data, and contain more detailed analyses of the variability of ground motion with region, event type and soil class. The new results have important implications for seismic-hazard analysis. The ground-motion relations predict that a great megathrust earthquake (**M** ≥8) at a fault distance of about 100 km would produce PSA on soil sites of about 110 cm/s^2 at 0.5 Hz, 660 cm/s^2 at 2.5 Hz and 410 cm/s^2 at 5 Hz, with a peak ground acceleration of about 18%g. These damaging levels of motion would be experienced over a very large area, corresponding to a rectangle about 300 km wide by 500 km long. Large in-slab events (**M** 7.5) would produce even higher PSA values within 100 km of the fault, but the in-slab motions attenuate much more rapidly with distance, greatly reducing the damage potential of events like the 2001 Nisqually, Washington earthquake, relative to a mega-thrust event. This is true not only for low-frequency ground motion, but even for 5 Hz. This suggests that the contemporary view of seismic hazard, namely that in-slab events dominate the hazard for 5 Hz for the 2% in 50 year probability level, may need revision. The hazard posed by moderate-to-large in-slab events such as the 2001 Nisqually earthquake is modest compared to that of a Cascadia mega-thrust earthquake of **M** ≥ 8, in terms of the area that would experience damaging levels of ground motion.

Analysis of regional variability of ground-motion amplitudes suggests that the use of regression equations based on a global subduction database is not well justified. In particular, amplitudes in

Cascadia differ by more than a factor of two from those in Japan for the same magnitude, distance, event type, and NEHRP soil class. This is believed to be due to regional differences in the depth of the soil profile, which are not captured by the NEHRP site classification scheme. Regional correction factors to account for these differences are proposed for Cascadia and Japan.

ACKNOWLEDGMENTS

We gratefully acknowledge the generous contributions of C.B. Crouse and Bob Youngs in making their subduction ground-motion databases available to us, Ralph Haugerud and Rob Williams for providing information about site classes for the region around Seattle, Washington, and Pat McCrory for discussions and information about whether the 1992 Cape Mendocino earthquake should be classified as an interface or a crustal earthquake. Art Frankel and Charles Mueller provided thoughtful reviews of the original manuscript. This work was supported by the U.S.G.S. National Earthquake Hazards Reduction Program under Grant 99HQGR0021. All figures were prepared using the graphics software package CoPlot (www.cohort.com).

REFERENCES

Abrahamson, N. and W. Silva (1997). Empirical response spectral attenuation relations for shallow crustal earthquakes. Seism. Res. L., **68**, 94-127.

Adams, J., D. Weichert and S. Halchuk (1999). Seismic hazard maps of Canada - 1999: 2%/50 Year values for selected Canadian cities. Geol. Survey of Canada Open File , 95pp. (www.seismo.nrcan.gc.ca)

Atkinson, G. (1997). Empirical ground motion relations for earthquakes in the Cascadia region. Can. J. Civil Eng., **24**, 64-77.

Atkinson, G. and R. Casey (2002). A comparative study of the 2001 Nisqually, Washington and Geiyo, Japan in-slab earthquakes. Draft manuscript for BSSA.

Atkinson, G. and J. Cassidy (2000). Integrated use of seismograph and strong motion data to determine soil amplification in the Fraser Delta: results from the Duvall and Georgia Strait earthquakes. Bull. Seism. Soc. Am., **90**, 1028-1040..

Atkinson, G. and W. Silva (2000). Stochastic modeling of California ground motions. Bull. Seism. Soc. Am., **90**, 255-274.

Boore, D. W. Joyner and T. Fumal (1997). Equations for estimating horizontal response spectra and peak acceleration from western North American earthquakes: A summary of recent work. Seism. Res. L., **68**, 128-153.

Boore, D. and W. Joyner (1997). Site amplifications for generic rock sites. Bull. Seism. Soc. Am., **87**, 327-341.

Chen, S. and G. Atkinson (2002). Global comparisons of earthquake source spectra. Bull. Seism. Soc. Am., **91**, in press.

Crouse, C. (1991). Ground-motion attenuation equations for Cascadia subduction zone earthquakes. Earthquake Spectra, **7**, 201-236.

Dobry, R., R. Borcherdt, C. Crouse, I. Idriss, W. Joyner, G. Martin, M. Power, E. Rinne and R. Seed (2000). New site coefficients and site classification system used in recent building seismic code provisions. Earthquake Spectra, **16**, 41-67.

Frankel, A., C. Mueller, T. Barnhard, D. Perkins, E. Leyendecker, N. Dickman, S. Hanson and M. Hopper (1996). National seismic hazard maps: Documentation June 1996. U.S. Geol. Surv. Open-file Rept. 96-532, 69 pp.

Heenan, S. (2002). Empirical study of the ground motion of earthquakes originating in the subduction zones of Japan and Cascadia. M.Sc. Thesis, Carleton University, Ottawa.

Joyner, W. and D. Boore (1993). Methods for regression analysis of strong motion data. Bull. Seism. Soc. Am., **83**, 469-487.

Joyner, W.B. and D.M. Boore (1994). Errata, Bull. Seism. Soc. Am., **84**, 955-956.

Oppenheimer, D., G. Beroza, G. Carver, L. Dengler, J. Eaton, L. Gee, F. Gonzalez, A. Jayko, W. H. Li, M. Lisowski, M. Magee, G. Marshall, M. Murray, R. McPherson, B. Romanowicz, K. Satake, R. Simpson, P. Somerville, R. Stein, and D. Valentine (1993). The Cape Mendocino, California, earthquakes of April 1992: Subduction at the triple junction, *Science* **261**, 433--438.

Wells, D. and K. Coppersmith (1994). New empirical relationships among magnitude, rupture length, rupture width, rupture area, and surface displacement. Bull. Seism. Soc. Am., **84**, 974-1002.

Williams, R.A., W.J. Stephenson, A.D. Frankel, and J.K. Odum (1999). Surface seismic measurements of near-surface P- and S-wave seismic velocities at earthquake recording stations, Seattle, Washington, *Earthquake Spectra* **15**, 565—583.

Youngs, R., S. Chiou, W. Silva and J. Humphrey (1997). Strong ground motion attenuation relationships for subduction zone earthquakes. Seism. Res. L., **68**, 58-73.

Appendix: Assigning NEHRP Site Classes for K-Net Stations

Shear-wave velocities have been determined for all but one K-Net station from measurements in boreholes (the exception is CHB023). Unfortunately, with one exception, the depths of all holes are between 10 and 20 m (the one exception is station AKT019, with a depth to bottom of 5.04 m). For this reason, the average velocity to 30 m, and therefore the NEHRP site classes, cannot be precisely determined for the K-Net stations. Rather than abandon the K-Net data, we assigned site classes based on a statistical approach, using data gathered by the U.S. Geological Survey from 69 boreholes in California.

A provisional NEHRP site class was assigned for each K-Net station by assuming that the velocity at the bottom of the associated borehole (Vbot) extends to 30m. Because velocities generally increase with depth, however, there is a finite chance that the velocities between the bottom of the borehole and 30 m are high enough that the NEHRP site class should be increased to a stiffer (faster) class. To account for this in a statistical way, we computed the ratio of Vbot to the effective constant velocity (Veff) from the bottom of the borehole to 30 m needed to raise the site class to the next stiffer class and then used the probability of the required Veff/Vbot, given the depth of the bottom of the K-Net borehole, to decide if the provisional site class should be changed. We derived a probability distribution for Veff/Vbot using data from 69 boreholes in California. Veff/Vbot from the 69 boreholes were computed for depths between 10 and 20 km, and then for each depth, the values of Veff/Vbot were tabulated in increments of 0.1 units, starting from 0.4, and a cumulative distribution was computed. A variety of functions were fit to the empirical distribution. A power law gave the best fit for Veff/Vbot > 1.0 (see Figure A1 for the empirical and power-law fits for depths of 10 and 20 m). The power-law distribution was then used to decide if the site class should be changed, given the K-Net borehole depth and the value of Veff/Vbot for that borehole.

A concrete example will help explain our procedure. Assume that the borehole at a particular Knet station was 14m deep, and that Veff/Vbot = 1.31 in order for the site class to change. Substituting 1.31 into the power law fit for 14m depth gives a cumulative percentage of 21% (21% of the California boreholes have a velocity that increases enough below 14m to give a V30 large enough to change the site class). We then decided whether or not to change the site class for each recording at that particular K-Net station by generating a random number between 0 and 1, and then multiplying that number by 100. If the resulting number was less that 21, we changed the site class. Using this procedure, we changed the site class for 89 out of 1001 stations. We are not claiming that the site classes assigned to the K-Net stations are correct for each station; this procedure only makes sense in a statistical way, when all the data are being thrown into a big pot without identifying each station.

We only consider cases when the velocity might have bumped the class into the next firmer class, not the other way, although as Figure A1 shows, there is a finite probability

that it could go the other way. The power-law fit is clearly invalid for cases where Veff/Vbot < 1 (as would be required to change to a softer site class), so in order to use the procedure above to reassign site to softer class, we would have to derive a different functional form. We decided that physically it is more likely that the site class would move to a stiffer rather than a softer class, and therefore we decided to retain the simplicity of the power law fit by only considering increases in site class.

The power-law distributions were only derived for borehole depths between 10m and 20m, and therefore they could not be used to assess the site class at the K-Net station AKT019, for which the borehole was only 5m deep. For this station, Veff/Vbot is so close to unity (1.23) that we changed the site class for this station (from D to C).

As mentioned before, the site classes at 89 out of 1001 stations were changed; this resulted in changes in site class for 441 of the 6307 K-Net recordings considered in the analysis in this paper. This seems reasonable.

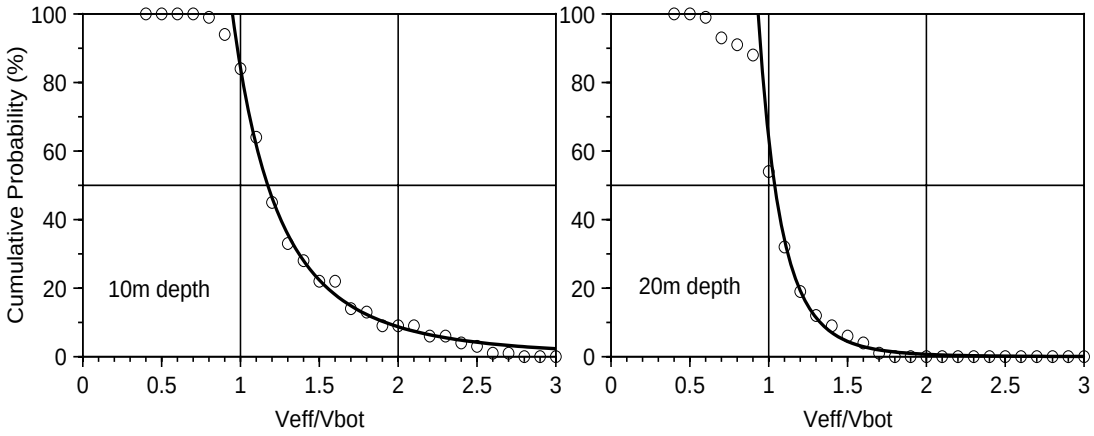

Figure A1. Cumulative probability of the ratio Veff/Vbot (see text) from 69 boreholes in California, for bottom depths of 10m and 20m. Also shown are the power-law fits to the observations.

Table 1 – Regression Coefficients

$\log Y = c_1 + c_2 \mathbf{M} + c_3 h + c_4 R - g \log R + c_5\, sl\, S_C + c_6\, sl\, S_D + c_7\, sl\, S_E$

where: Y is peak ground acceleration (PGA) or 5% damped pseudo-acceleration (PSA) in cm/s^2, random horizontal component

M = moment magnitude (use **M**=8.5 for interface events of **M**>8.5, **M**=8.0 for in-slab events of **M**≥8)

h = focal depth in km, $R = \sqrt{(D_{fault}^2 + \Delta^2)}$ with D_{fault} = closest distance to fault surface, in km (use h=100 km for events with depth > 100 km)

$\Delta = 0.00724\ 10^{0.507\,\mathbf{M}}$

S_C=1 for NEHRP C soils (360<β≤760 m/s), =0 otherwise

S_D=1 for NEHRP D soils (180≤β≤360 m/s), =0 otherwise

S_E=1 for NEHRP E soils (β<180 m/s), =0 otherwise

$g = 10^{(1.2 - 0.18\,\mathbf{M})}$ for interface events, $g = 10^{(0.301 - 0.01\,\mathbf{M})}$ for in-slab events

sl = 1. for PGArx≤ 100 cm/s^2 OR frequencies ≤ 1 Hz

sl = 1. – (f-1) (PGArx-100.)/400. for 100.<PGArx<500. cm/s^2 (1 Hz<f<2 Hz)

sl = 1. - (f-1) for PGArx≥500. cm/s^2 (1 Hz<f<2 Hz.)

sl = 1. – (PGArx-100.)/400. for 100.<PGArx<500. cm/s^2 (f≥2 Hz)

sl = 0. for PGArx≥500. cm/s^2 (f≥2 Hz)

PGArx = predicted PGA on rock (NEHRP B), in cm/s^2

σ = standard deviation of residuals = $\sqrt{(\sigma_1^2 + \sigma_2^2)}$ where 1, 2 denote estimated intra-event and inter-event variability, respectively.

Coefficients for Interface events:

freq	c1	c2	c3	c4	c5	c6	c7	σ	σ_1	σ_2
0.33	2.301	0.02237	0.00012	0.000	0.10	0.25	0.36	0.36	0.31	0.18
0.5	2.1907	0.07148	0.00224	0.000	0.10	0.25	0.40	0.34	0.29	0.18
1	2.1442	0.1345	0.00521	-0.00110	0.10	0.30	0.55	0.34	0.28	0.19
2.5	2.5249	0.1477	0.00728	-0.00235	0.13	0.37	0.38	0.29	0.25	0.15
5	2.6638	0.12386	0.00884	-0.00280	0.15	0.27	0.25	0.28	0.25	0.13
10	2.7789	0.09841	0.00974	-0.00287	0.15	0.23	0.20	0.27	0.25	0.10
25	2.8753	0.07052	0.01004	-0.00278	0.15	0.20	0.20	0.26	0.22	0.14
PGA	2.991	0.03525	0.00759	-0.00206	0.19	0.24	0.29	0.23	0.20	0.11

Coefficients for In-slab events:

0.33	-3.70012	1.1169	0.00615	-0.00045	0.10	0.25	0.36	0.30	0.29	0.08
0.5	-2.39234	0.9964	0.00364	-0.00118	0.10	0.25	0.40	0.30	0.28	0.11
1	-1.02133	0.8789	0.00130	-0.00173	0.10	0.30	0.55	0.29	0.27	0.11
2.5	0.005445	0.7727	0.00173	-0.00178	0.13	0.37	0.38	0.28	0.26	0.10
5	0.51589	0.69186	0.00572	-0.00192	0.15	0.27	0.25	0.28	0.26	0.10
10	0.43928	0.66675	0.01080	-0.00219	0.15	0.23	0.20	0.28	0.27	0.07
25	0.50697	0.63273	0.01275	-0.00234	0.15	0.20	0.20	0.25	0.24	0.07
PGA	-0.04713	0.6909	0.01130	-0.00202	0.19	0.24	0.29	0.27	0.23	0.14

Note: The c1 coefficient may be refined to better model the Japan or Cascadia region, as described in the text. The revised c1 values specific to Japan and Cascadia are listed in Table 3.

Table 2 – Mean Residuals (log units) for Records of M≥6.0 within 100 km of the fault

a) Interface Events

Case	No. records	0.5Hz	1.0Hz	2.5Hz	5.0Hz	10. Hz	Std. Error
Overall	194	0.04	0.05	0.07	0.07	0.17	0.03
By Magnitude							
6.0≤**M**<6.6	30	-0.04	-0.02	0.24	0.34	0.43	0.05
6.6≤**M**<7.2	87	0.15	0.11	0.09	0.06	0.19	0.03
7.2≤ **M** ≤7.7	30	-0.11	0.01	-0.13	-0.07	-0.01	0.05
7.7≤ **M** ≤8.3	47	-0.01	0.01	0.03	0.02	0.10	0.04
By Site Class							
A/B	93	-0.02	-0.02	0.04	-0.04	0.17	0.03
C	35	0.28	0.25	0.21	0.24	0.17	0.05
D	62	-0.01	0.04	0.02	0.13	0.18	0.04
E	4	0.17	0.05	0.07	0.25	0.14	0.15
By Region							
Cascadia[1]	14	0.39	0.23	0.07	0.18	0.07	0.08
Japan	39	0.04	0.08	0.09	0.27	0.25	0.05
Other Pacific[2]	125	-0.08	-0.05	0.02	-0.03	0.14	0.03

Notes: 1. Cascadia interface is entirely the Cape Mendocino event (crustal?)
2. Other Pacific includes Alaska, Mexico, Central and South America.
3. Std. Error lists typical standard error of the mean residuals (all frequencies).

b) In-slab Events

Case	No. records	0.5Hz	1.0Hz	2.5Hz	5.0Hz	10.Hz	Std. Error
Overall	302	0.03	0.05	0.08	0.06	-0.02	0.02
By Magnitude							
6.0≤**M**<6.6	24	0.03	0.12	0.15	0.14	0.00	0.06
6.6≤**M**<7.2	264	0.03	0.05	0.07	0.06	-0.02	0.02
7.2≤**M**≤7.7	14	-0.12	-0.01	0.03	-0.09	-0.06	0.08
By Site Class							
A/B	24	-0.02	-0.06	0.09	0.17	0.12	0.06
C	158	0.05	0.09	0.10	0.06	-0.02	0.02
D	88	-0.02	0.02	0.05	0.05	-0.02	0.03
E	32	0.08	0.01	0.04	-0.02	-0.16	0.05
By Region							
Cascadia	162	0.19	0.11	0.07	-0.03	-0.19	0.02
Japan	136	-0.07	0.05	0.12	0.21	0.20	0.03
Other Pacific	20	-0.10	-0.03	0.02	-0.01	0.03	0.06

Table 3 – Recommended Regional Ground Motion Correction Factors (log units)

Frequency (Hz)	Factor: Cascadia	Factor: Japan	C_1 interface (Cascadia)	C_1 interface (Japan)	C_1 in-slab (Cascadia)	C_1 in-slab (Japan)
0.33	0.06	-0.03	2.36	2.27	-3.64	-3.73
0.5	0.14	-0.05	2.33	2.14	-2.25	-2.44
1.0	0.04	0.04	2.18	2.18	-0.98	-0.98
2.5	-0.02	0.06	2.50	2.58	-0.01	0.07
5.	-0.12	0.18	2.54	2.84	0.40	0.70
10.	-0.28	0.17	2.50	2.95	0.16	0.61
25.	-0.28	0.17	2.60	3.05	0.23	0.68
pga	-0.20	0.15	2.79	3.14	-0.25	0.10

Table 4 – Residual Statistics After Application of Regional Correction Factors

	Interface M≥7.5 at Dfault<300km			**In-slab M≥6.5 at Dfault<100km**	
Frequency (Hz)	Mean residual	Standard deviation		Mean residual	Standard deviation
0.33	-0.09	0.36		-0.15	0.23
0.5	-0.02	0.33		-0.03	0.23
1.	0.03	0.31		0.01	0.25
2.5	-0.05	0.26		0.06	0.26
5.	-0.01	0.28		0.04	0.23
10.	0.01	0.30		0.05	0.25
25.	-0.06	0.26		-0.04	0.23
pga	0.00	0.24		0.01	0.23

FIGURE CAPTIONS

1. Database for subduction zone earthquakes. Top frame shows data available for interface events, by NEHRP site class. Lower frame shows data available for in-slab events, by NEHRP site class. Data for moment magnitude <5.4 are not shown. Magnitude-distance range of most engineering interest is shaded dark grey. Magnitude-distance cut-offs imposed on final regressions are shaded light grey. KNET data that are believed to be unreliable at higher frequencies (moderate magnitudes at large distances; see text) are not included.
2. Slope of log Y' versus log R for records within 50 to 300 km of the fault plane, where Y' = PSA(0.5 or 1 Hz) exp(0.001 R) and R is average distance to the fault as defined by Equation 1. Plotted slopes are obtained as the average values for 0.5 and 1 Hz, for data within a 1 unit magnitude bin. For example the values plotted at **M** 6.5 are the slopes for interface (open squares) and in-slab (filled squares) data of $6.0 \leq \mathbf{M} < 7.0$. The lines show the adopted slopes for the final regressions.
3. Illustration of the difference in attenuation behavior of interface events versus in-slab events. Plot shows 1-Hz PSA data for interface events of **M** 8±0.3 (left) in comparison to 1-Hz PSA data for in-slab events of **M** 7±0.3 (right).
4. Soil amplification factors for NEHRP site classes C and D relative to rock (NEHRP B), as given by regression coefficients c_5, c_6 and c_7 (linear), respectively. The linear factors apply for $PGA_{rx} \leq 100$ cm/s^2. Amplifications for stronger ground motions (250 cm/s^2) are also shown. For $PGA_{rx} \geq 500$ cm/s^2, soil and rock motions are the same for f>2 Hz.
5. Scaling of ground motion amplitudes with moment magnitude for interface events (h=20 km) in the distance range (closest distance to fault) from 10 to 50 km. Filled symbols show data for rock (NEHRP A,B), while open symbols show data for soil (NEHRP C, D, E). Solid lines show scaling behavior using quadratic term in magnitude, while dashed lines show behavior using linear term in magnitude, both for rock sites at a distance of 20 km.
6. Scaling of ground motion amplitudes with moment magnitude for interface events (h=20 km) in the distance range (closest distance to fault) from 70 to 150 km. Filled symbols show data for rock (NEHRP A,B), while open symbols show data for soil (NEHRP C, D, E). Solid lines show scaling behavior using quadratic term in magnitude, while dashed lines show behavior using linear term in magnitude, both for rock sites at a distance of 100 km.
7. Scaling of ground motion amplitudes with moment magnitude for in-slab events (h=50 km) in the distance range (closest distance to fault) from 20 to 70 km. Filled symbols show data for

rock (NEHRP A,B), while open symbols show data for soil (NEHRP C, D, E). Solid lines show scaling behavior using quadratic term in magnitude, while dashed lines show behavior using linear term in magnitude, both for rock sites at a distance of 40 km.

8. Scaling of ground motion amplitudes with moment magnitude for in-slab events (h=50 km) in the distance range (closest distance to fault) from 70 to 150 km. Filled symbols show data for rock (NEHRP A,B), while open symbols show data for soil (NEHRP C, D, E). Solid lines show scaling behavior using quadratic term in magnitude, while dashed lines show behavior using linear term in magnitude, both for rock sites at a distance of 100 km.
9. Peak ground acceleration for rock (NEHRP A/B) and soil (NEHRP D) for interface events (h=20 km) of **M** 5.5, 6.5, 7.5 and 8.5 (top frame) and in-slab events (h=50 km) of **M** 5.5, 6.5 and 7.5. Nonlinear soil response is assumed for records with PGA_{rx}>100 cm/s^2.
10. Comparison of response spectra amplitudes at frequencies 0.5 Hz (top frame) and 5 Hz (lower frame), for interface (h=20 km) and in-slab (h=50 km) events of **M** 6.5 on NEHRP D soil sites. The corresponding predictions of Youngs et al. (1997) for interface (open symbols) and in-slab (filled symbols) events are also shown. Interface ground motions for **M** 8.5 (NEHRP D) are also shown in comparison to the Youngs et al. (1997) predictions.
11. Log residuals (=log observed value – log predicted value) based on regression equation, for interface events. The residuals from the Cape Mendocino event (discussed in text) are denoted with an asterisk.
12. Log residuals (=log observed value – log predicted value) based on regression equation, for in-slab events.
13. Variability (standard deviation of log residuals) of ground motion estimates. Triangles show variability for interface events, while squares show variability for in-slab events. Open symbols used for events of **M** 6 to 7.2, with filled symbols for larger events.
14. Comparison of amplitudes predicted by our regression equations for rock (abR) and NEHRP D soil (abD) to observed amplitudes, for rock, C, D and E data, for interface events (h=20 km) of **M** 8 ± 0.3. Corresponding predictions of Youngs et al. for rock (y97R) and soil (y97S) are also shown.
15. Comparison of amplitudes predicted by our regression equations for rock (abR) and soil (abD) to observed amplitudes, for rock, C, D and E data, for in-slab events (h=50 km) of **M** 6.8 ± 0.3. Corresponding predictions of Youngs et al. for rock (y97R) and soil (y97S) are also shown.

16. Predicted spectra for earthquakes of **M** 6.2 (top frames), 7.2 (middle frames) and 8.0 (lower frames), at distances of 50 km (left) and 100 km (right) from the fault, for NEHRP C site conditions, for interface (solid lines) and in-slab (dashed lines) events. Corresponding predictions for shallow California earthquakes (from Atkinson and Silva, 2000) are denoted by lines with 'C'.
17. Correction factors to account for regional differences in ground motion amplitudes. Factors are the average residual (in log units) for all records of **M**≥6 within 100 km of the fault, within a given region (symbols). Heavy lines show average residual for these records over all regions.
18. Replotted residuals for in-slab events at frequencies of 0.5 and 5 Hz, after correcting the Cascadia and Japan equations using the factors of Table 3.

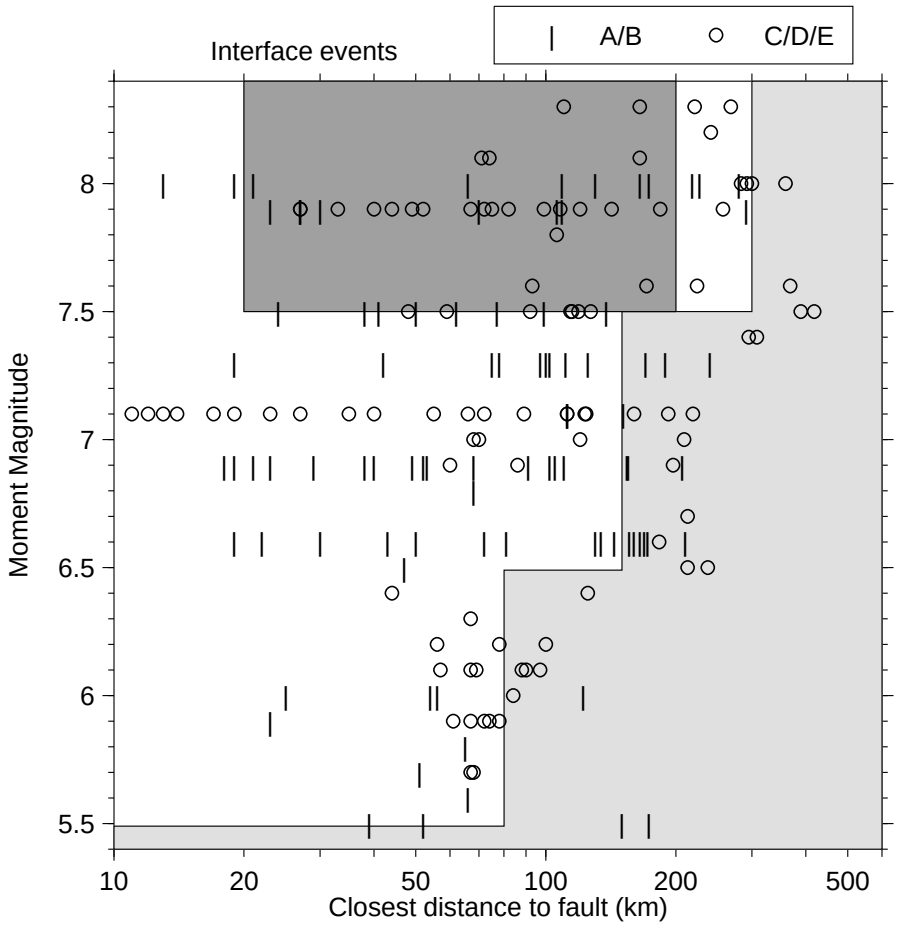

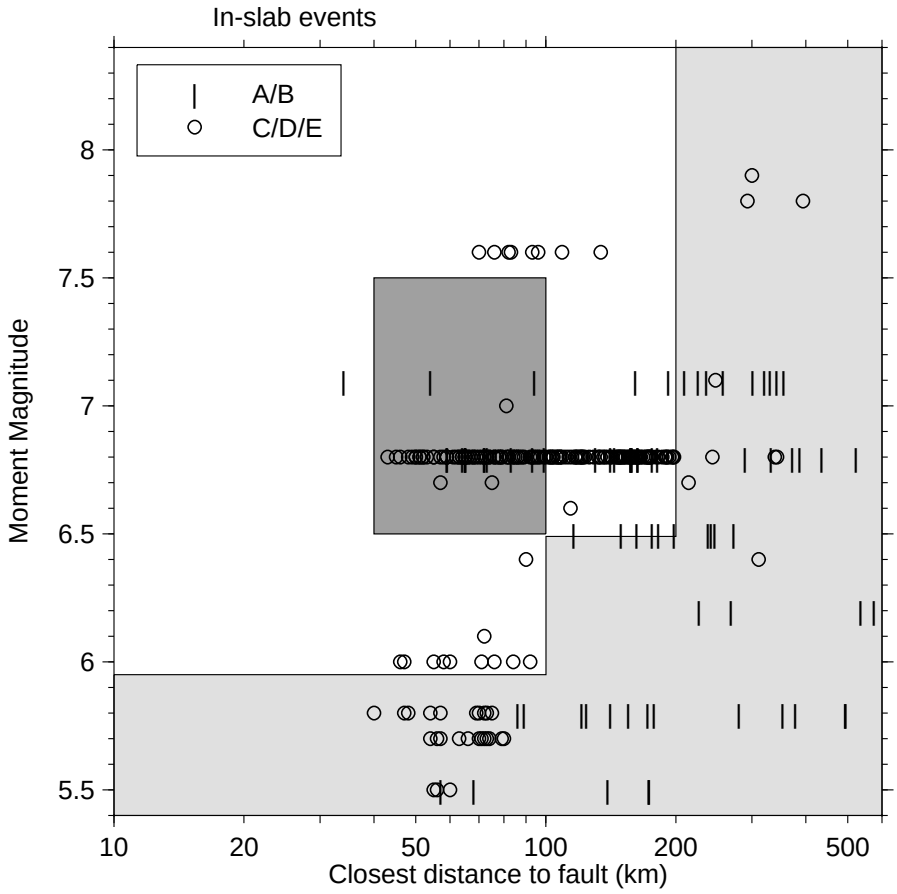

File: C:\GAIL\ab02\magdist.draw; Date: 2002-06-13

Fig. 01

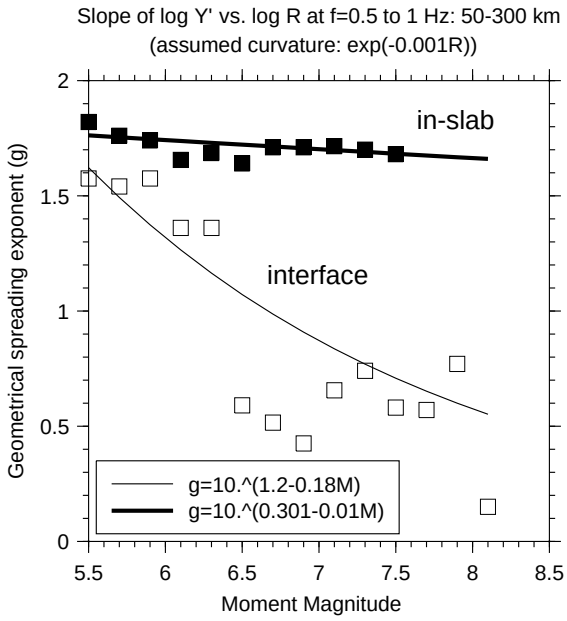

File: C:\GAIL\ab02\slope_dmb.draw; Date: 2002-04-24

Fig. 02

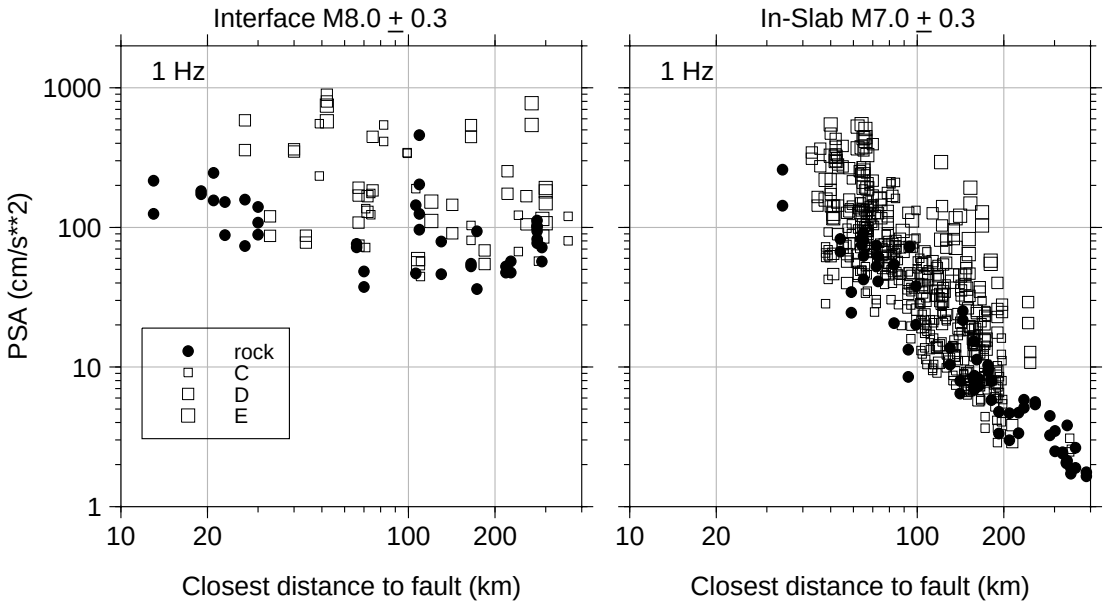

File: C:\GAIL\ab02\sub_80_sla_70.draw; Date: 2002-04-26

Fig. 03

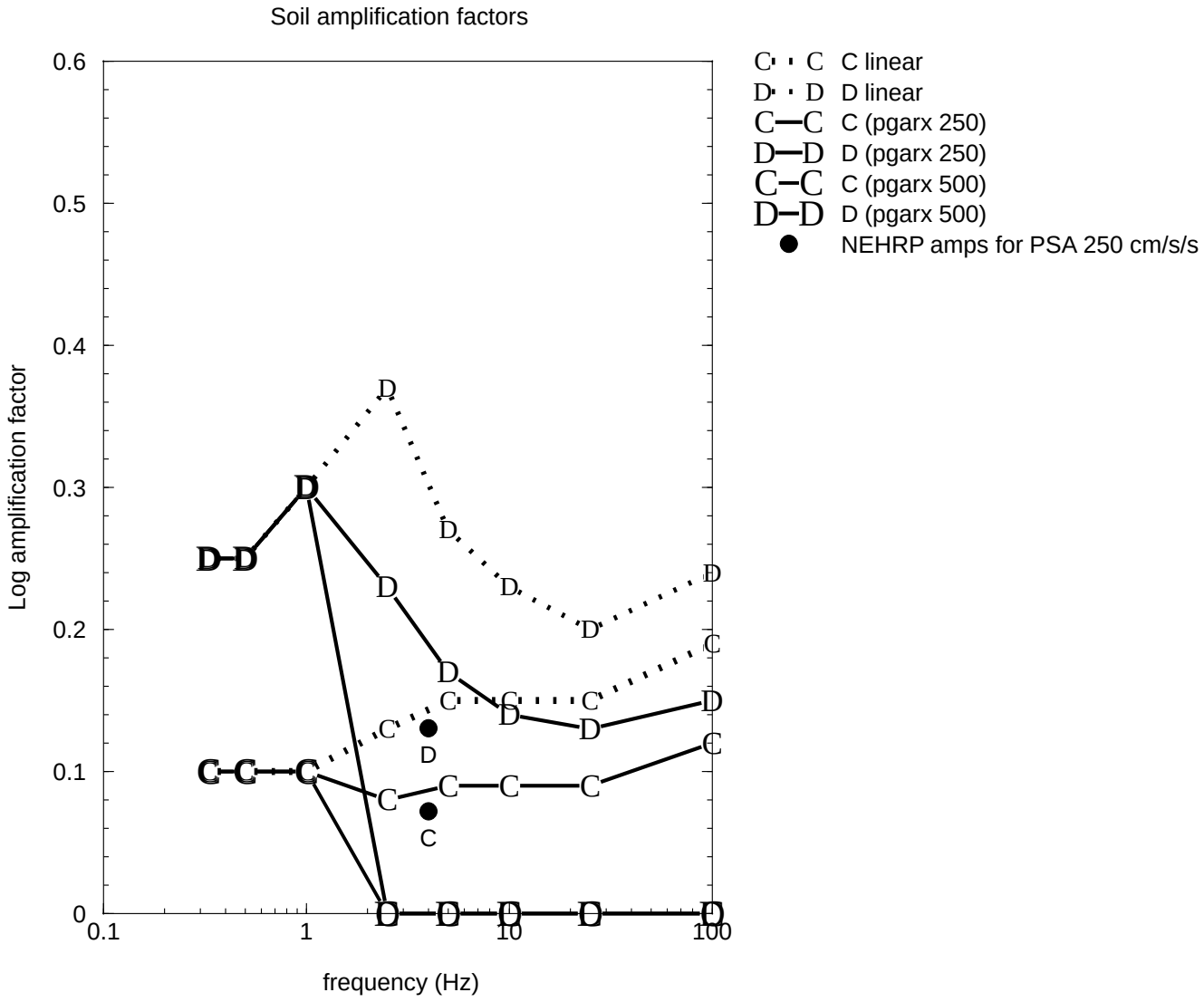

File: C:\GAIL\ab02\soilplot.draw; Date: 2002-04-29

Fig. 04

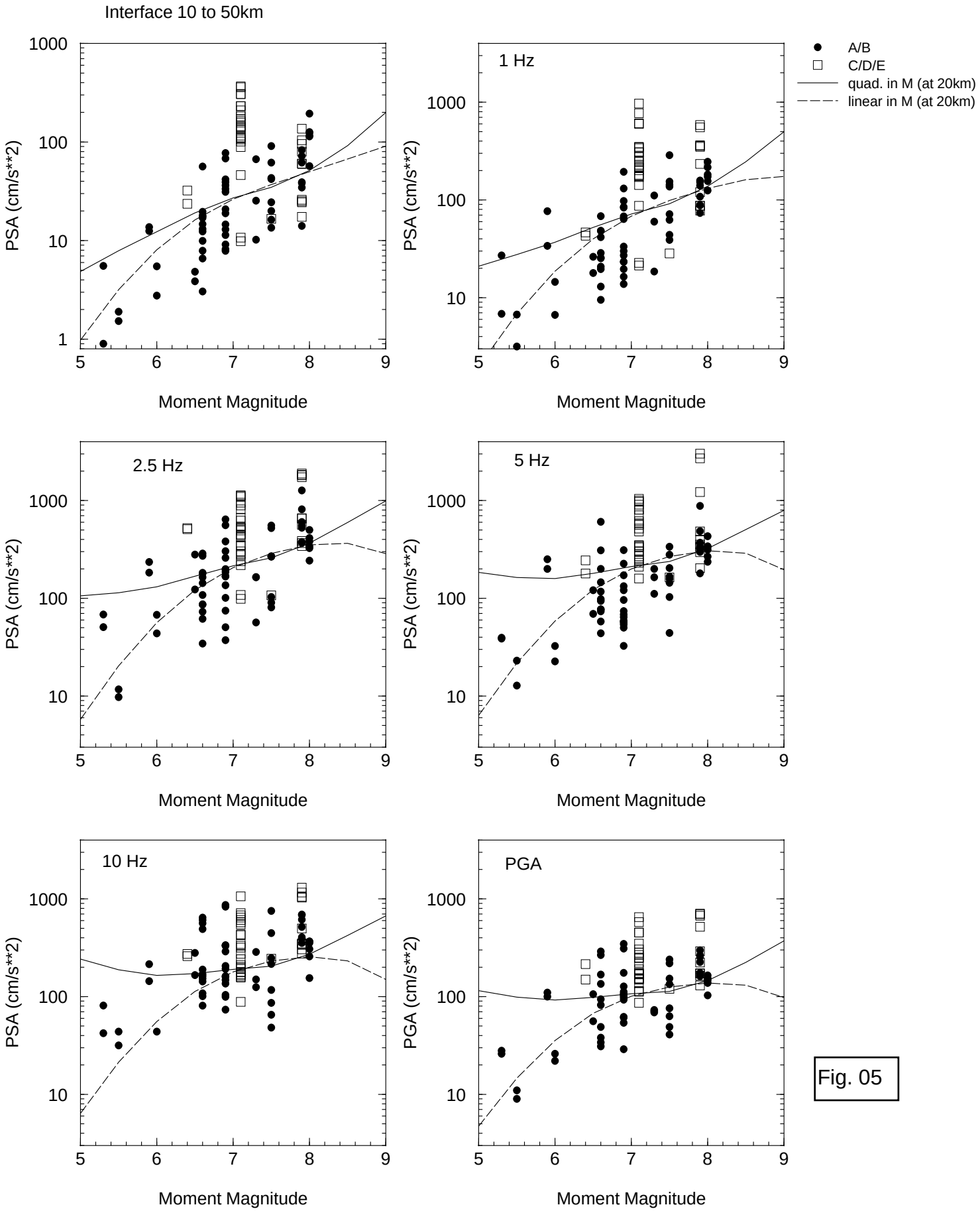

Fig. 05

File: C:\WINDOWS\Desktop\mywork\MAXLIK\eqndat\mscale0n.draw; Date: 2002-08-02

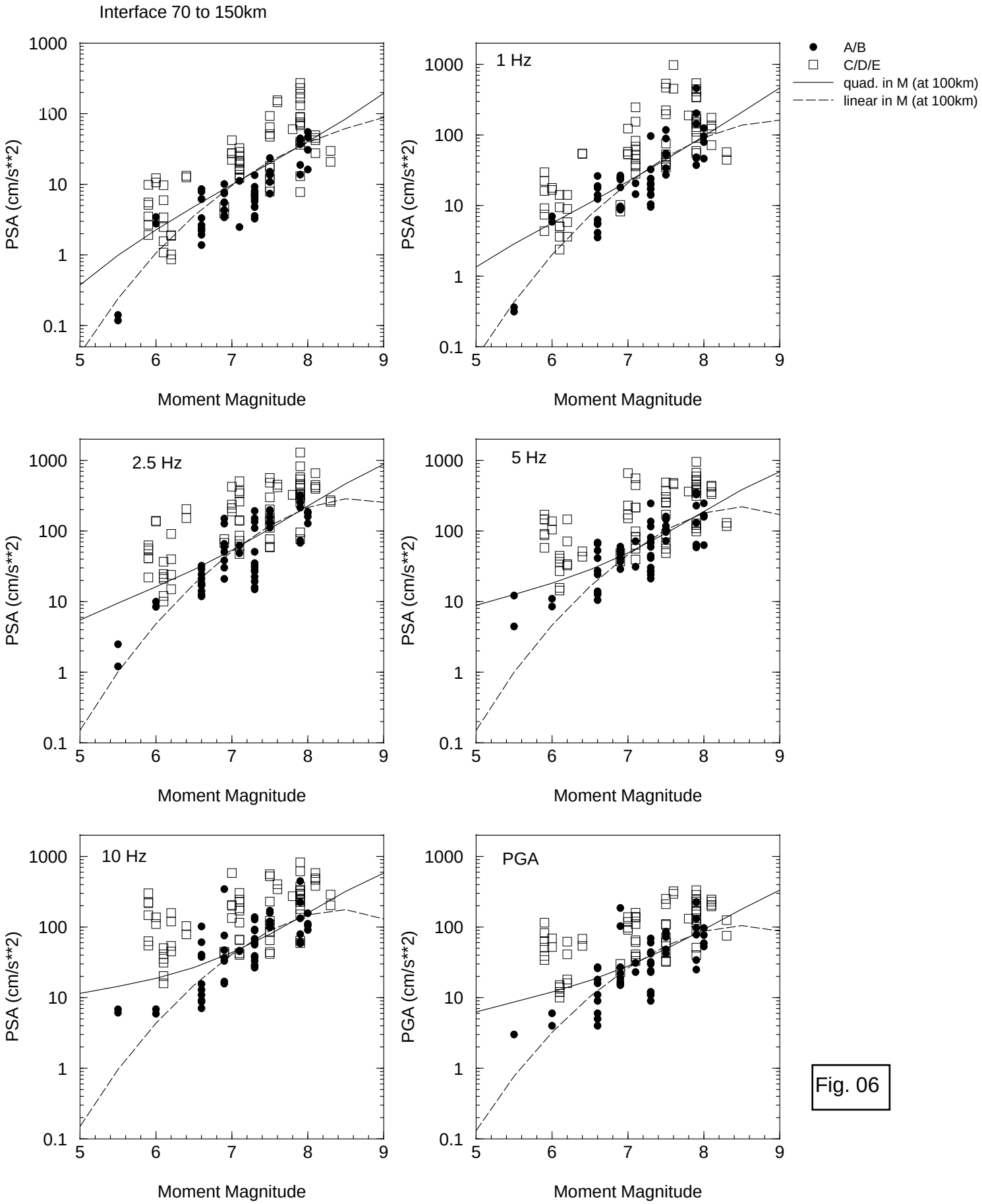

Fig. 06

File: C:\WINDOWS\Desktop\mywork\MAXLIK\eqndat\mscale0f.draw; Date: 2002-08-02

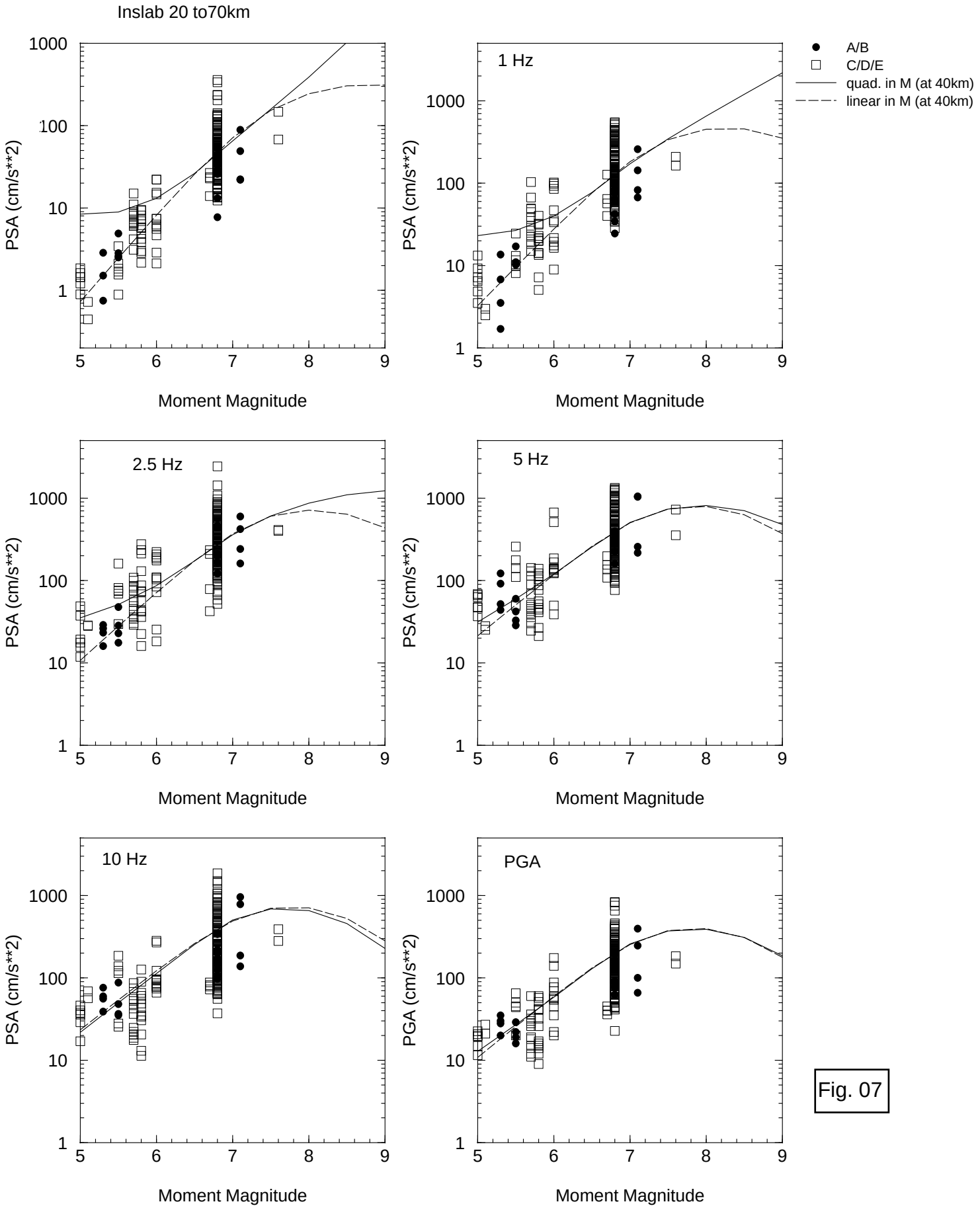

Fig. 07

File: C:\WINDOWS\Desktop\mywork\MAXLIK\eqndat\mscale1n.draw; Date: 2002-08-02

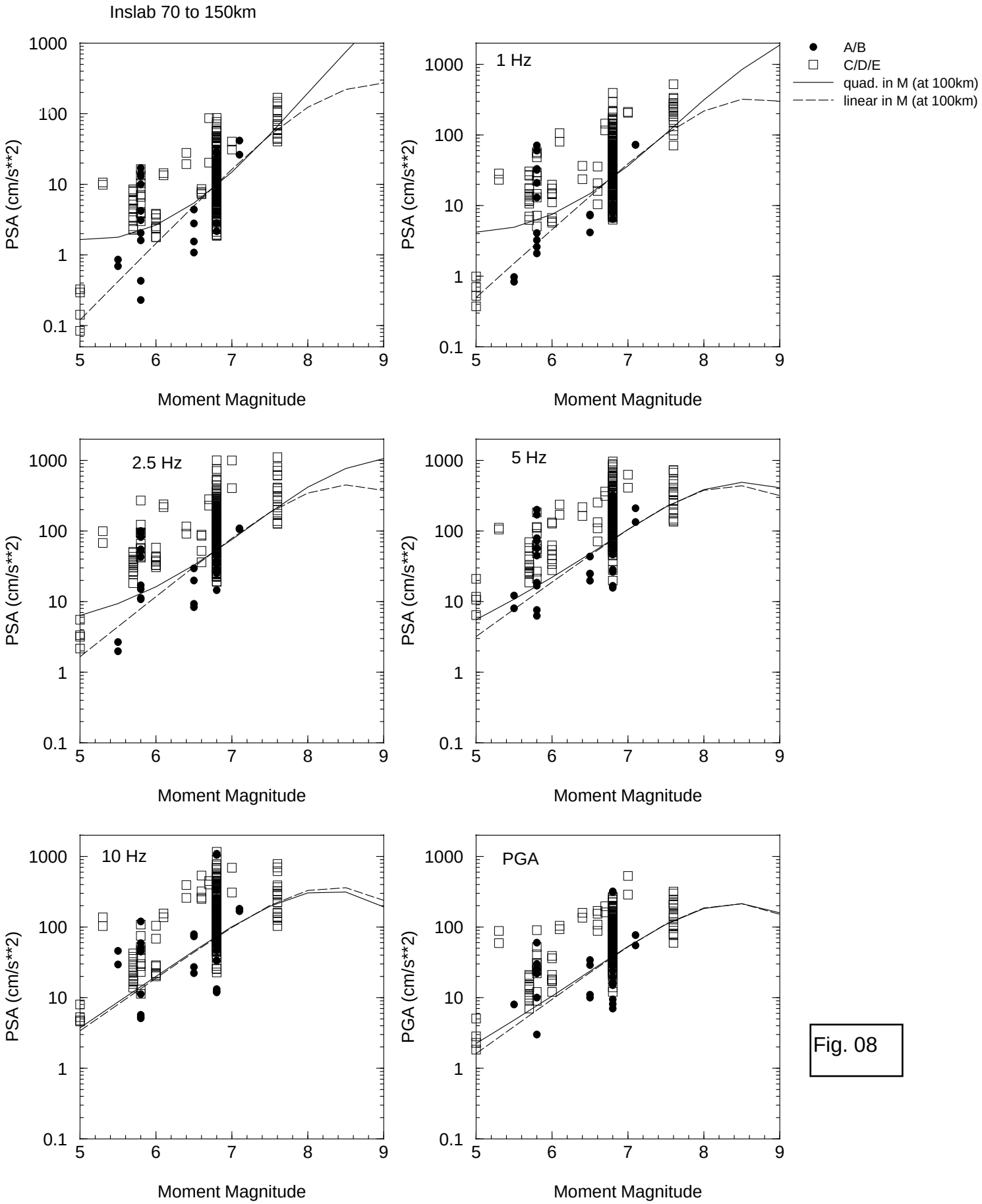

Fig. 08

File: C:\WINDOWS\Desktop\mywork\MAXLIK\eqndat\mscale1f.draw; Date: 2002-08-02

PGA on Rock vs. NEHRP D

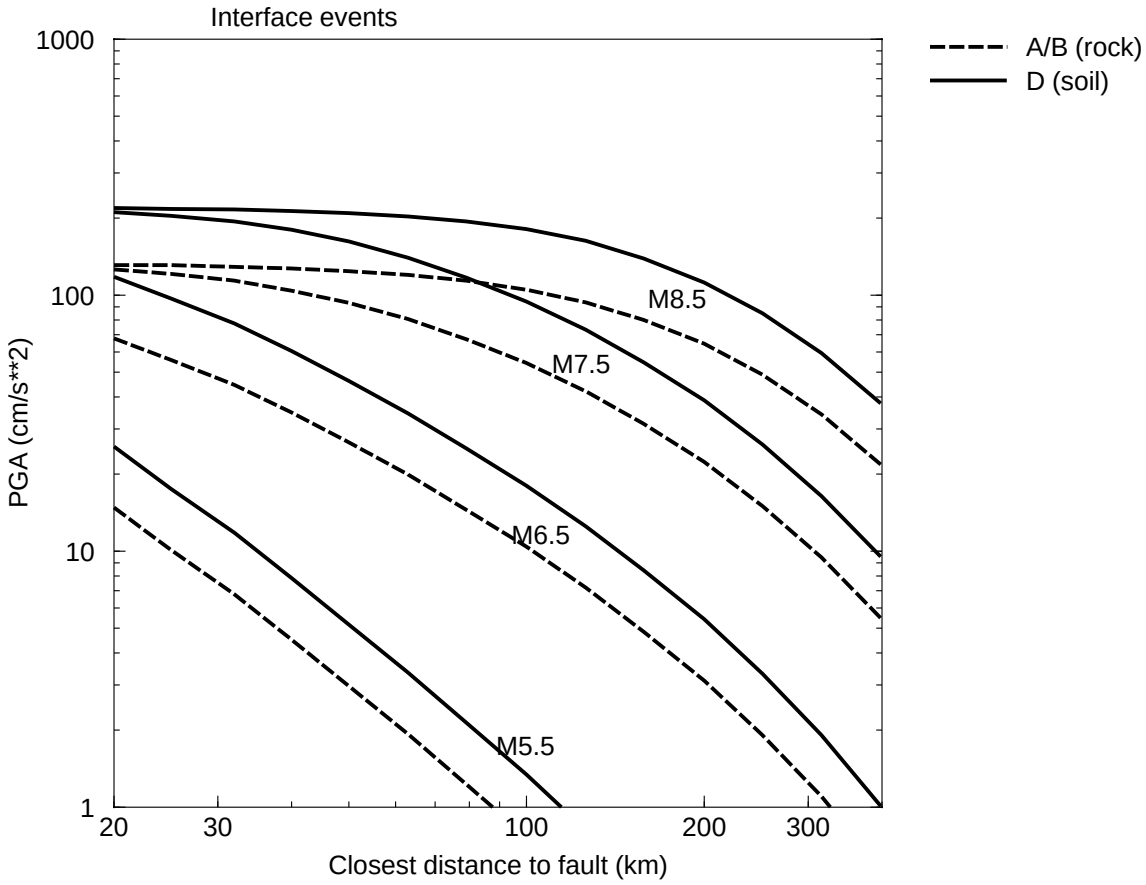

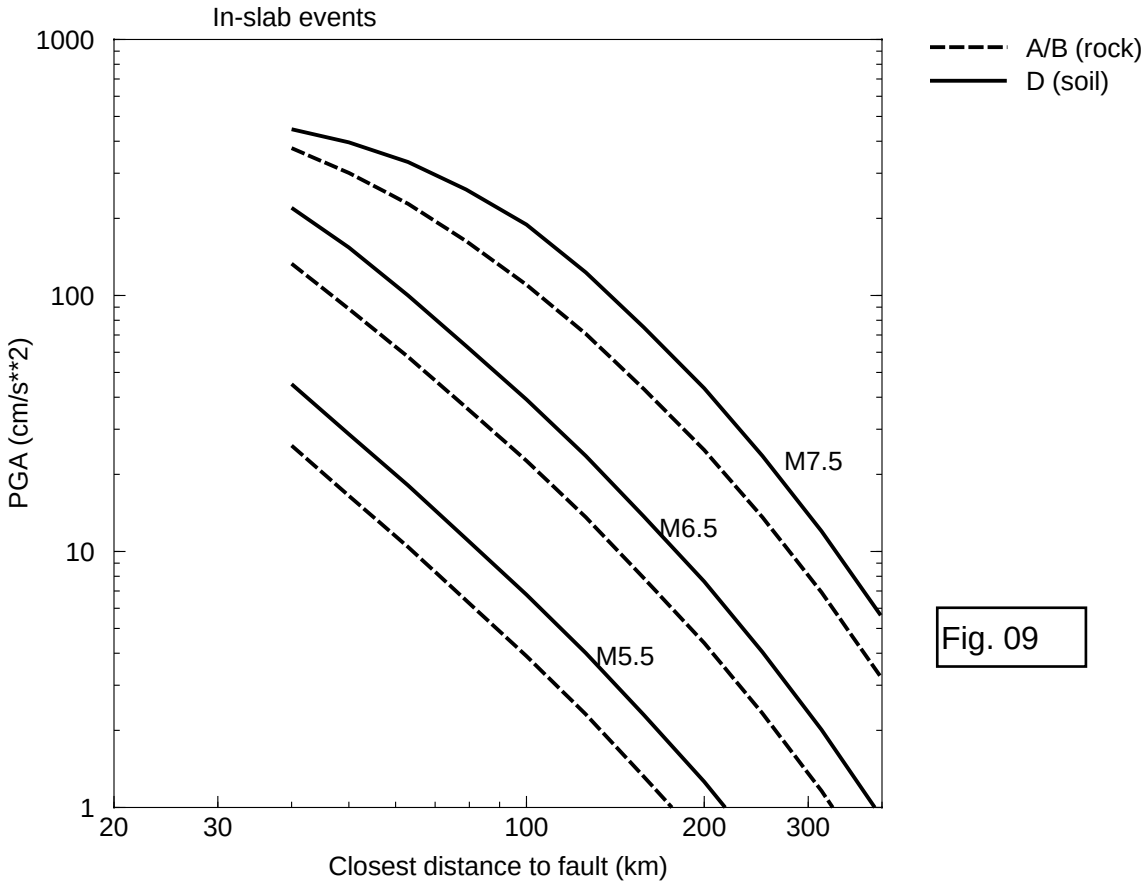

Fig. 09

File: C:\WINDOWS\Desktop\mywork\MAXLIK\eqndat\pga.draw; Date: 2002-06-24

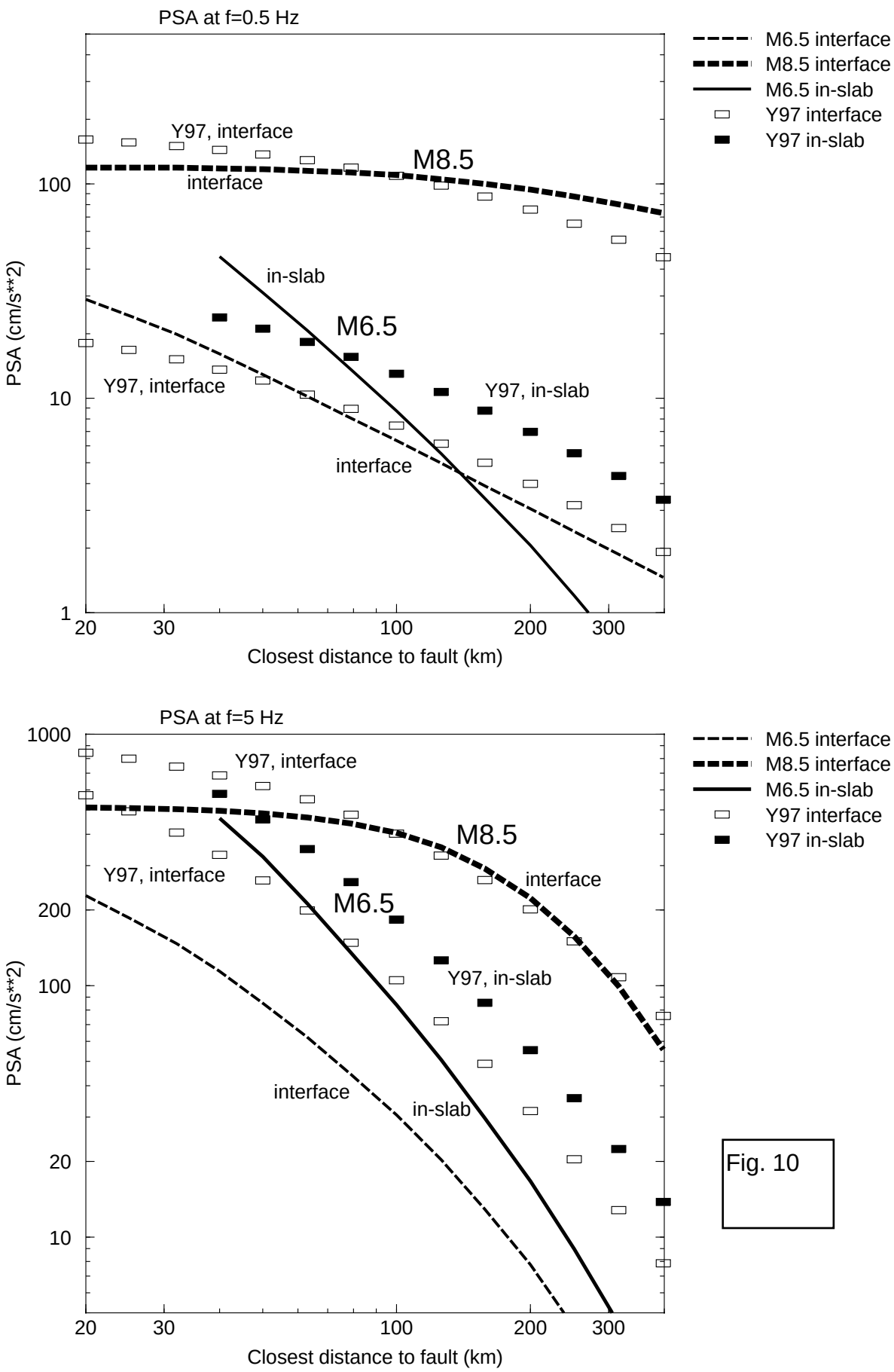

Fig. 10

File: C:\WINDOWS\Desktop\mywork\MAXLIK\eqndat\attend.draw; Date: 2002-06-25

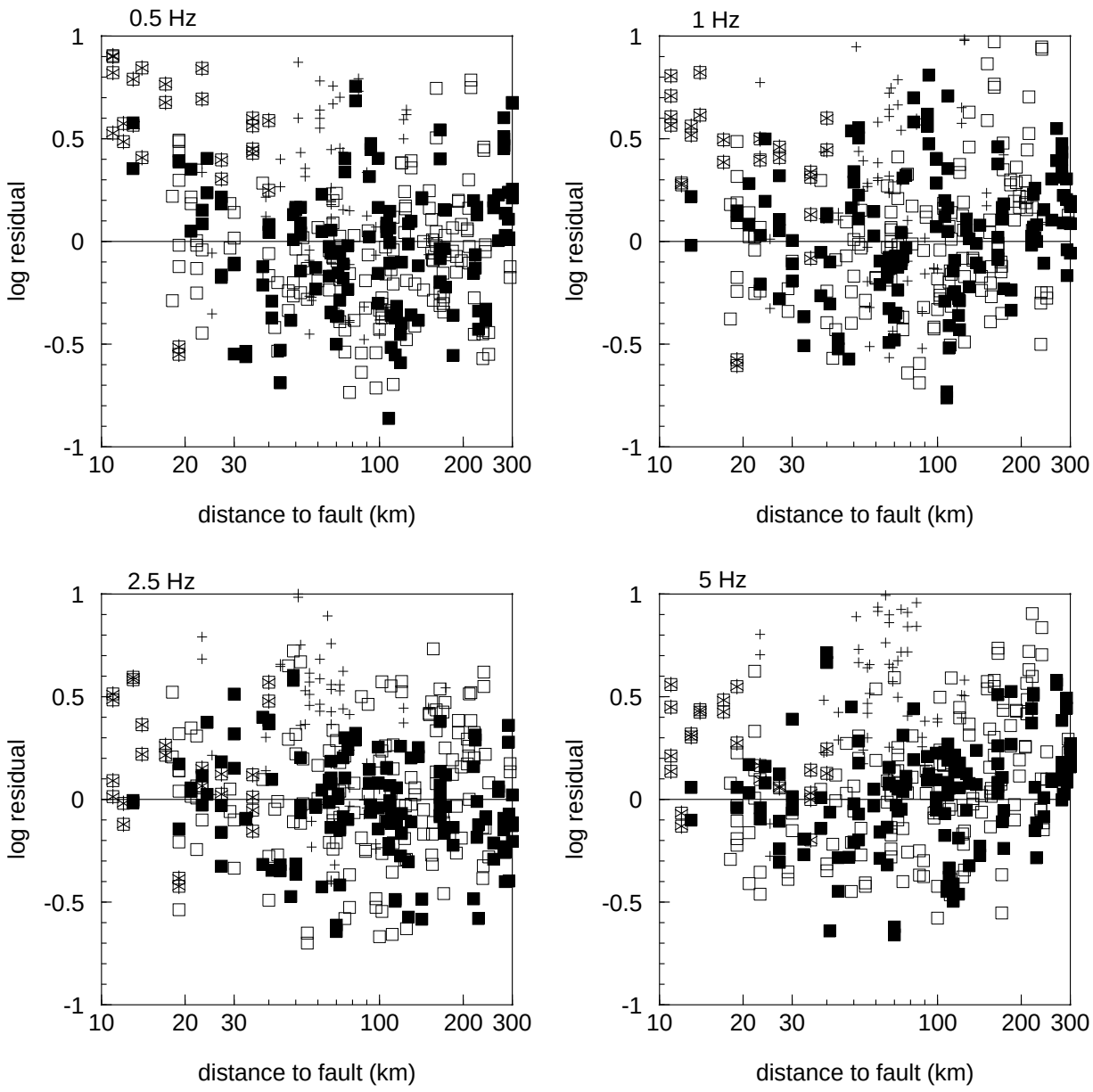

e: C:\WINDOWS\Desktop\mywork\MAXLIK\resplot\RESALL0.draw; Date: 2002-06-11

Fig. 11

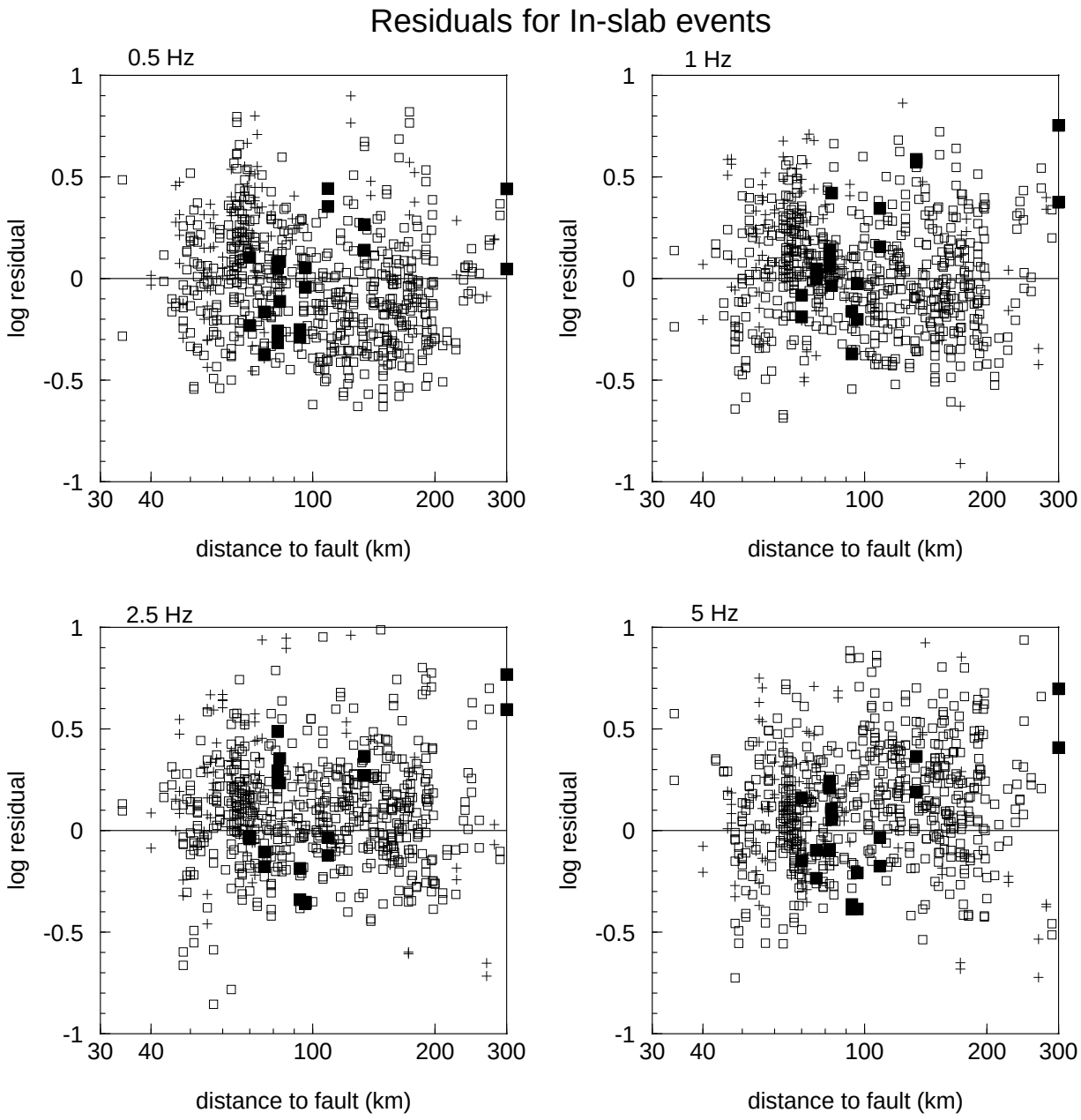

e: C:\WINDOWS\Desktop\mywork\MAXLIK\resplot\RESALL1.draw; Date: 2002-06-11

Fig. 12

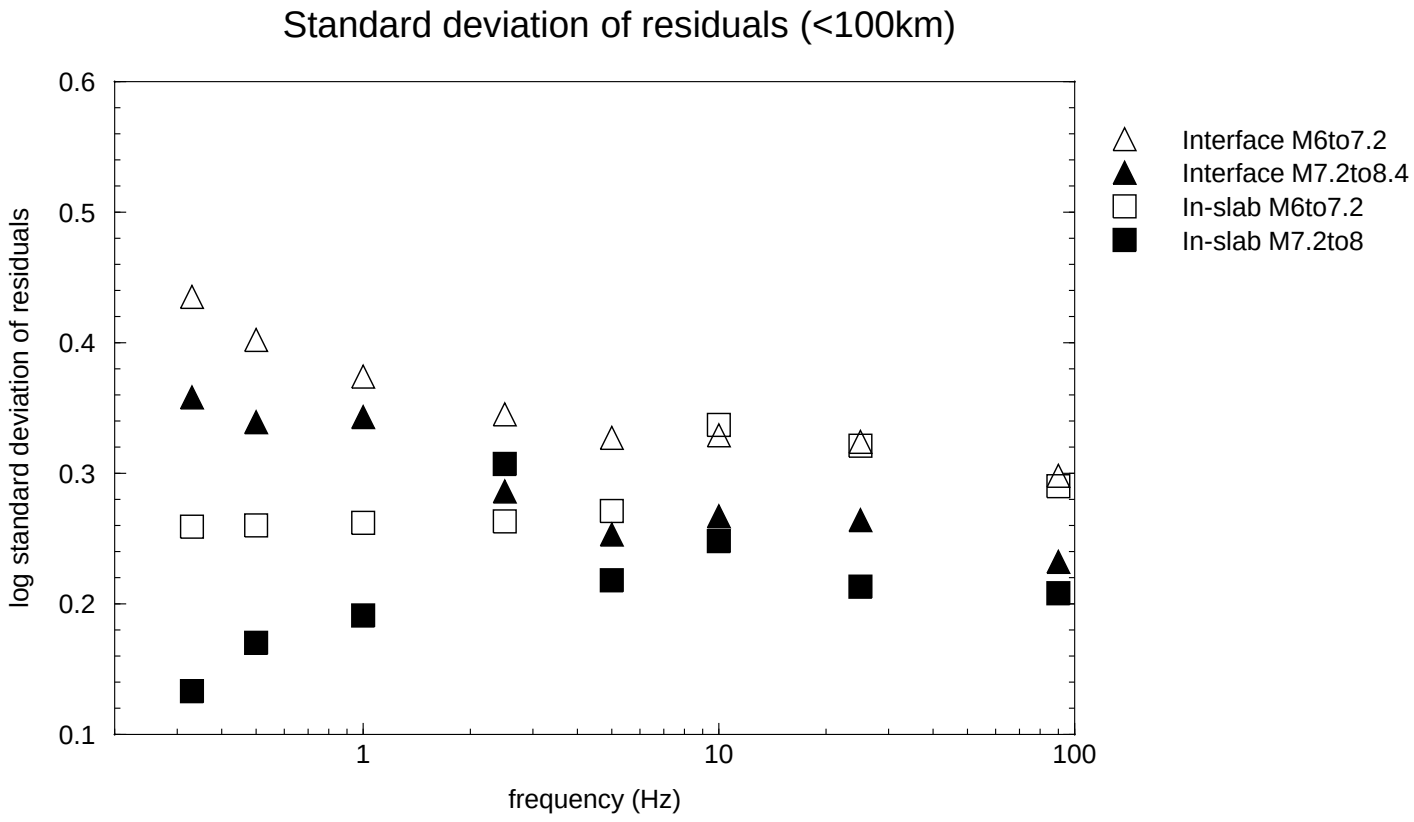

File: C:\WINDOWS\Desktop\mywork\MAXLIK\resplot\stdres2.draw; Date: 2002-06-07

Fig. 13

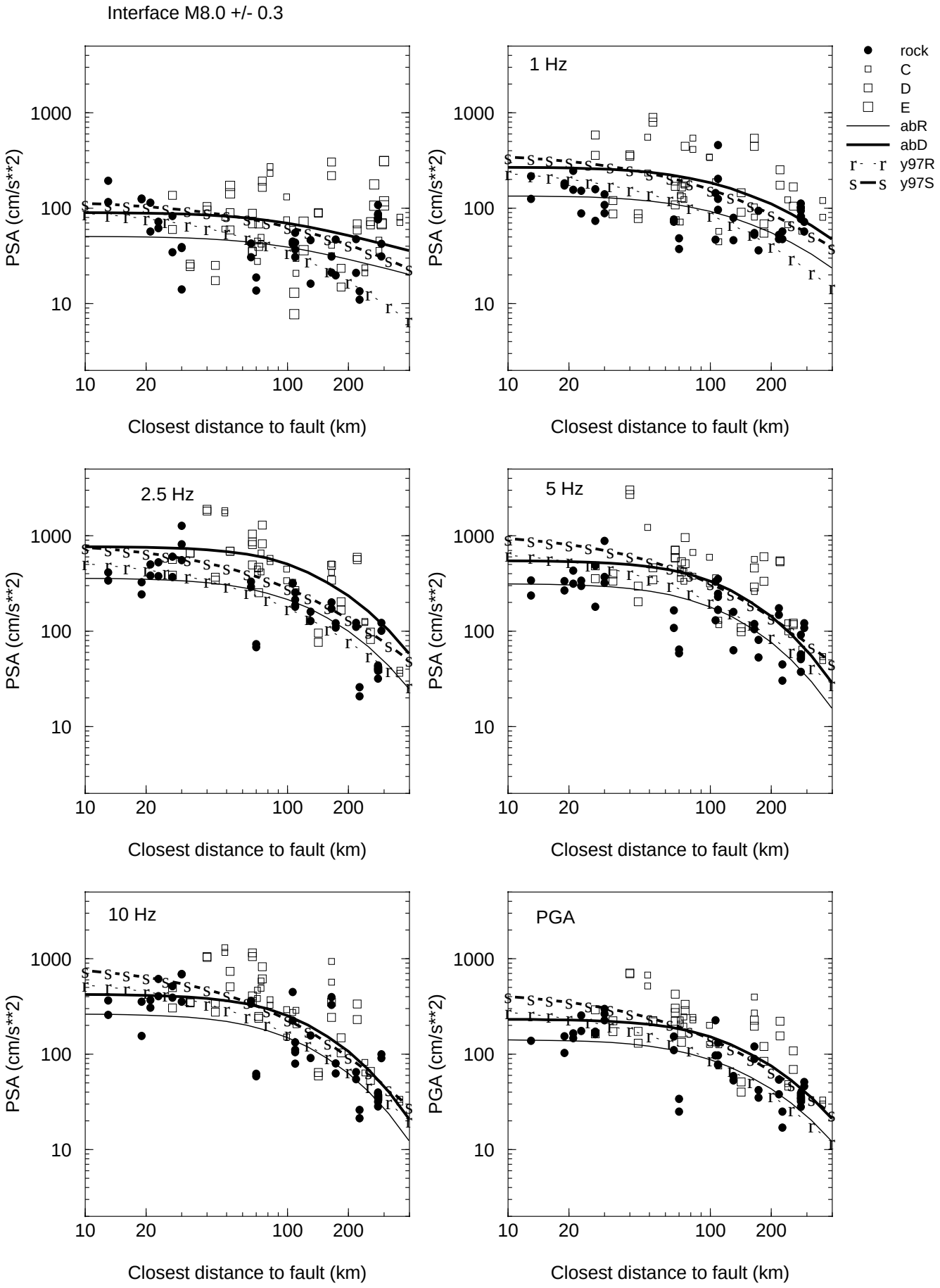

File: C:\WINDOWS\Desktop\mywork\MAXLIK\eqndat\dbase9.draw; Date: 2002-06-01

Fig. 14

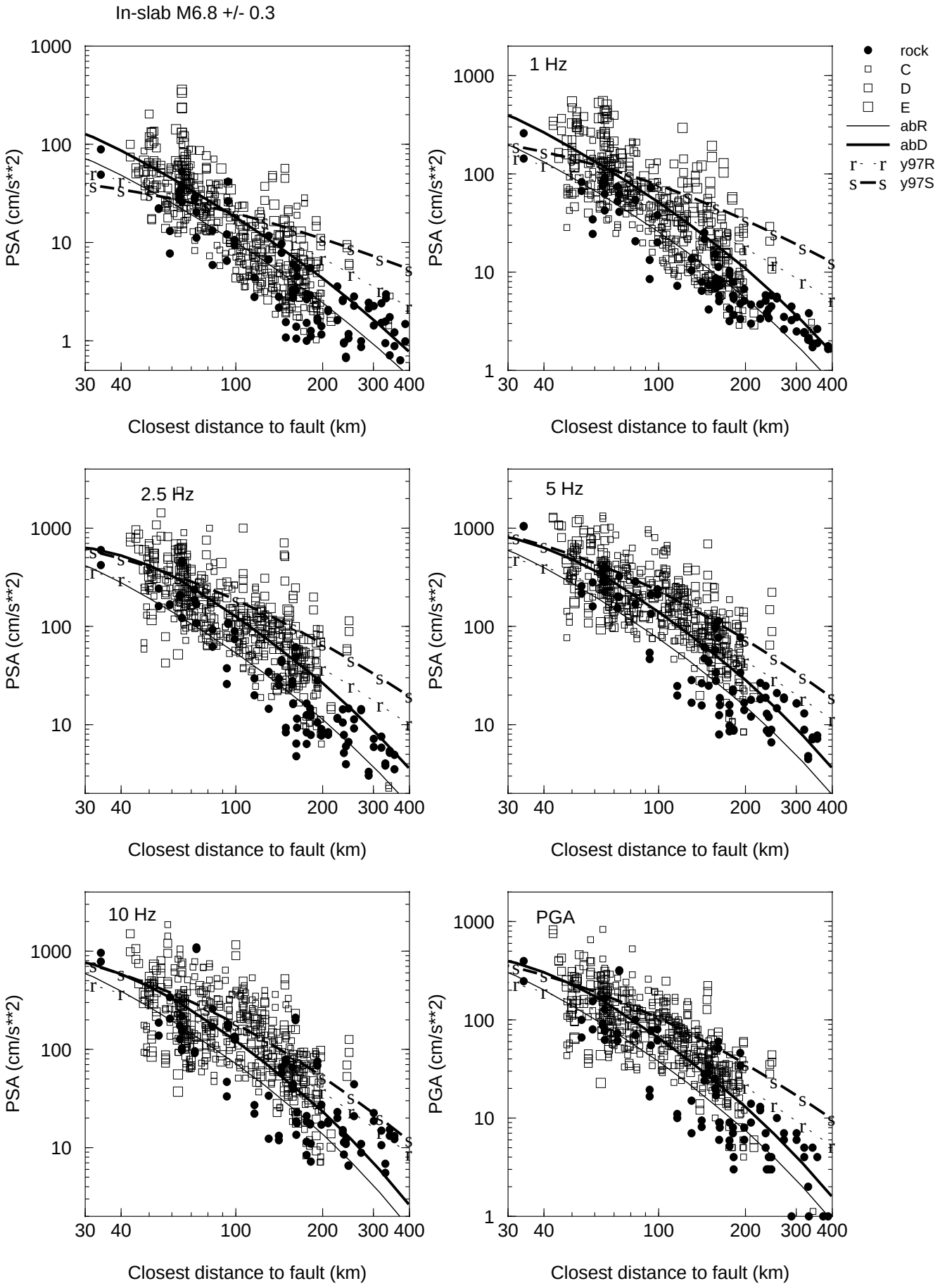

File: C:\WINDOWS\Desktop\mywork\MAXLIK\eqndat\dbase6.draw; Date: 2002-06-01

Fig. 15

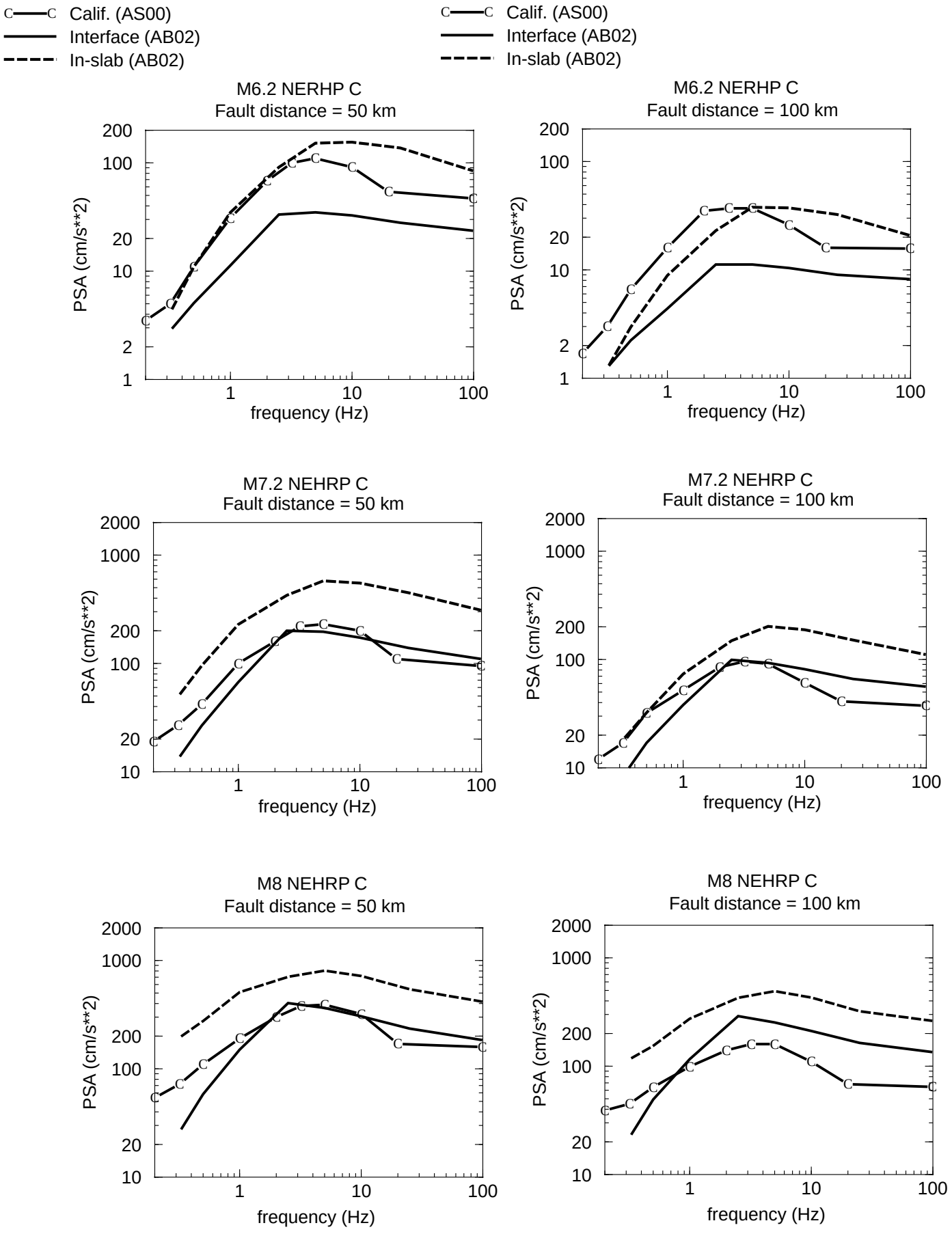

File: C:\WINDOWS\Desktop\mywork\MAXLIK\eqndat\spectra2.draw; Date: 2002-06-09

Fig. 16

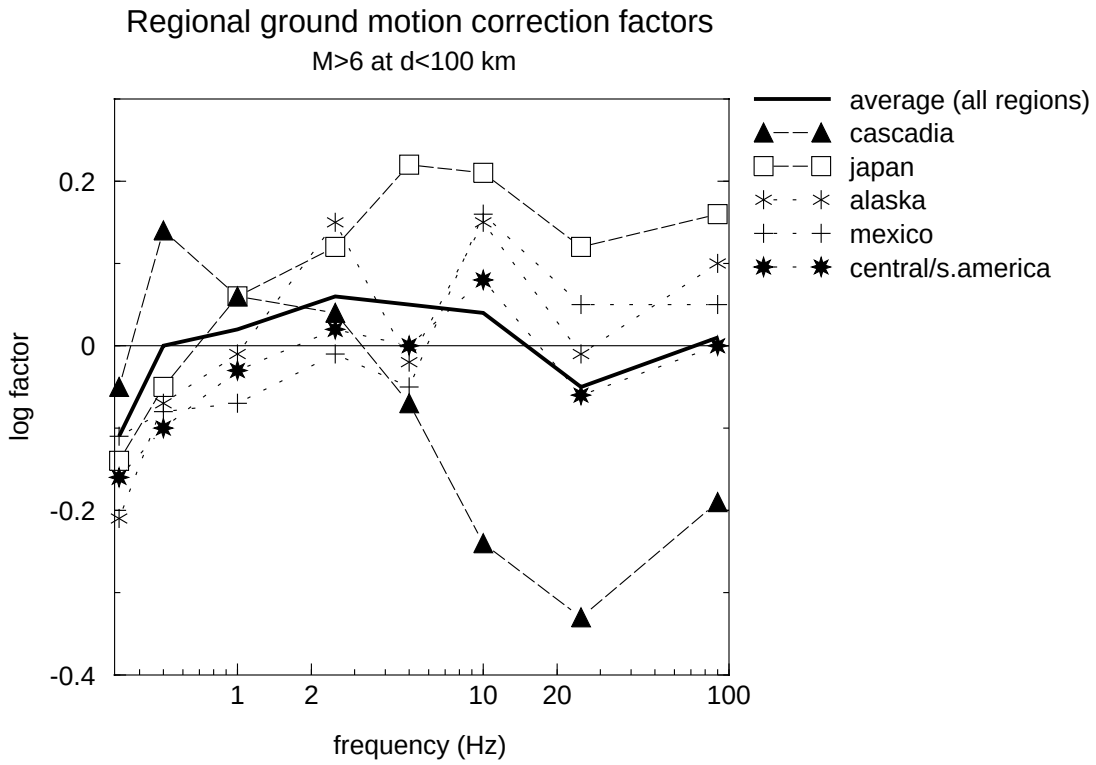

File: C:\WINDOWS\Desktop\mywork\MAXLIK\REGFACSUM.draw;Date: 2002-06-10

Fig. 17

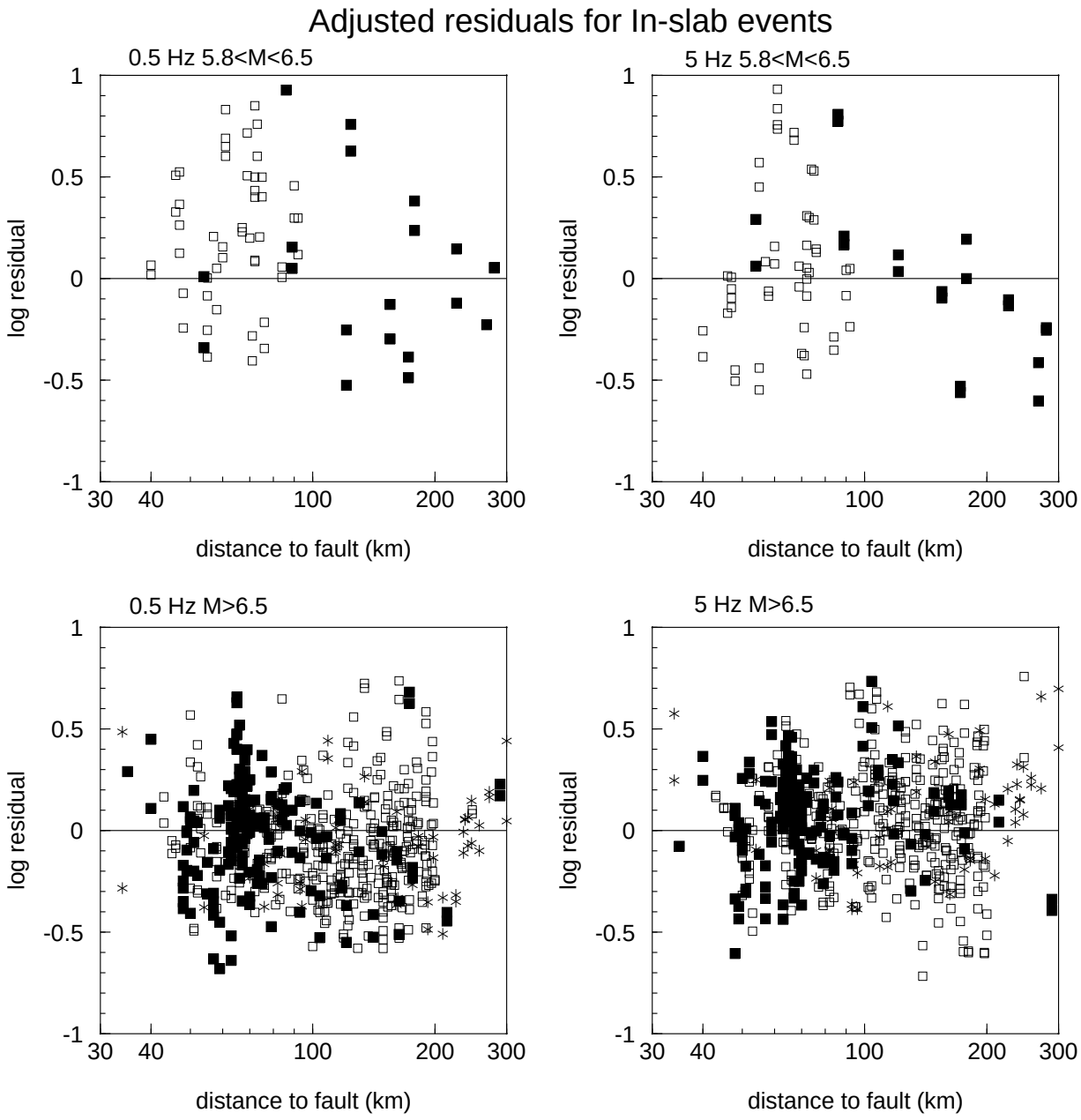

File: C:\WINDOWS\Desktop\mywork\MAXLIK\resplot\resadj1.draw; Date: 2002-06-11

Fig. 18